The effects of meteoric diagenesis on the geochemical composition and microstructure of Pliocene fossil *Terebratalia coreanica* and *Laqueus rubellus* brachiopod shells from northeastern Japan

Hiroshi Fujioka[1], Hideko Takayanagi[1], Koshi Yamamoto[2] and Yasufumi Iryu[1*]

Abstract

Stable carbon (δ^{13}C) and oxygen isotope (δ^{18}O) compositions of fossil brachiopod shells can be used to interpret paleoclimatic and paleoceanographic conditions. However, the initial isotopic composition of the living shells might be modified by diagenetic alteration. To assess the degree of this modification, we analyzed δ^{13}C and δ^{18}O and three common indicators of alteration in shells: minor element (manganese (Mn), iron (Fe), and strontium (Sr)) concentrations; cathodoluminescence (CL)/non-luminescence; and the shell microstructure of fossil *Terebratalia coreanica* and *Laqueus rubellus* (rhynchonellate brachiopod) shells from an exposure of conglomerates of the Tentokuji Formation (Pliocene, 3.85–2.75 Ma) in northeastern Japan. Two indices were used to quantify the preservation state of shell microstructure: the altered fiber ratio (AFR) and the altered fiber and puncta-filling cement ratio (AF-PCR). We qualified the degree of luminescence by measuring the mean cathodoluminescence index (MCLI), defined as the mean R values in a particular area of a CL image with RGB colors. The δ^{13}C and δ^{18}O values were negatively correlated with AFR or AF-PCR and MCLI. The sampling spots with high Mn and Fe concentrations also exhibited relatively low δ^{13}C and δ^{18}O. The δ^{13}C and δ^{18}O were more strongly correlated with Mn concentration than with Fe concentration. Therefore, of the three minor elements examined in this study, Mn concentration is the most reliable indicator of meteoric diagenesis in the studied shells. Unlike Mn and Fe concentrations, Sr concentrations in the modern and fossil brachiopod shells were similar, with overlapping ranges. This indicates that Sr concentration is not likely to be a good indicator of diagenetic alteration in the studied shells. Our study provides further evidence that multiple criteria should be applied and cross-checked when assessing diagenetic alteration of brachiopod shells.

Keywords: Brachiopod, Carbon isotopes, Oxygen isotopes, Minor element concentration, Cathodoluminescence, Meteoric diagenesis, *Terebratalia coreanica*, *Laqueus rubellus*, Pliocene, Japan

* Correspondence: yasufumi.iryu.d8@tohoku.ac.jp
[1]Department of Earth Science, Graduate School of Science, Tohoku
University, Sendai 980-8578, Japan
Full list of author information is available at the end of the article

Introduction

Stable carbon isotope (δ^{13}C) and oxygen isotope (δ^{18}O) compositions of biogenic carbonates are useful for paleoenvironmental analysis. The δ^{13}C and δ^{18}O values of shells from brachiopods belonging to the subphylum Rhynchonelliformea (Williams et al. 1996; hereafter, simply called brachiopods) have been widely used for reconstructing paleoclimatic and paleoceanographic conditions during the Phanerozoic, and especially during the Paleozoic (e.g., Veizer et al. 1999), because of (1) their widespread occurrence in marine sediment and their continuous geologic record; (2) their low-magnesium calcite mineralogy, which is less susceptible to diagenetic alteration than high-magnesium calcite and aragonite; and (3) shell secretion in isotopic equilibrium with ambient seawater (Lowenstam 1961). The disequilibrium effects of shell fractionation have been very well investigated since Lowenstam (1961), and it is understood in detail which taxa and shell portions reliably record past ocean environments with the highest fidelity (Auclair et al. 2003; Yamamoto et al. 2010a, 2010b, 2011, 2013; Cusack et al. 2012; Takayanagi et al. 2012, 2013, 2015).

To evaluate the preservation of brachiopod shells, the following three screening criteria have been commonly applied (Ullmann and Korte 2015): (1) minor element (manganese (Mn), iron (Fe), and strontium (Sr)) concentrations, which vary with diagenetic alteration; (2) luminescence/non-luminescence with "cold cathode"; and (3) shell microstructures observed via scanning electron microscope (SEM). Well-preserved shells or shell portions are non-luminescent, having high Sr and low Mn and Fe concentrations and well-preserved microstructure.

However, these techniques do not work effectively in all cases. It has been shown that there might be no significant difference in the isotopic composition between well-preserved and diagenetically altered shells determined using the minor element concentrations (e.g., Bruckschen et al. 1999; Korte et al. 2005). Some unaltered modern brachiopod shells show bright cathodoluminescence (CL) images (e.g., Barbin and Gaspard 1995; Griesshaber et al. 2007), which is usually taken to be an indication of diagenetic alteration. The δ^{13}C and δ^{18}O values of luminescent and non-luminescent shells might overlap or be similar in range (Rush and Chafetz 1990; Mii et al. 1997, 2013; Yamamoto et al. 2017). Therefore, applying multiple criteria to assess the diagenetic alteration and cross-checking them are required to distinguish between diagenetically altered and unaltered brachiopod shells (Yamamoto et al. 2017).

The isotopic and minor element signatures in carbonate minerals vary with the isotopic and chemical composition of the ambient pore water (Wenzel 2000; Ullmann et al. 2014), which can be marine, meteoric, or hydrothermal water, or various mixtures of these. This variation implies that diagenetic modification of the chemical and isotopic composition in brachiopod shells embedded in carbonate deposits is likely to be different from that in siliciclastic and volcaniclastic deposits. Cathodoluminescence images of brachiopod carbonates might not be useful for detecting diagenetic alteration where sources of Mn (the activator for CL) are very limited. There are some instances showing that the δ^{13}C and δ^{18}O values or the preservation of shell microstructure are unrelated with CL intensity (Yamamoto et al. 2017).

To better understand the impact of diagenetic modification on the isotopic and chemical composition of brachiopod shells in siliciclastic deposits, we examined the δ^{13}C and δ^{18}O values, minor element concentrations, CL images, and shell microstructure of fossil brachiopod shells of two species, *Terebratalia coreanica* (Adams and Reeve 1850) (Family Terebrataliidae Richardson 1975) and *Laqueus rubellus* (Sowerby 1846) (Family Laqueidae Thomson 1927) collected from the conglomerates of the Pliocene Tentokuji Formation in Minehama, northeastern Japan. We compared these shells with modern shells from Otsuchi Bay (northeastern Japan) and Sagami Bay (central Japan). *Terebratalia coreanica* is generally found at water depths of 13–287 m in the northwestern Pacific Ocean (Hokkaido, Tsugaru Strait to Boso Peninsula on the Pacific side, Korean Strait north to Tsugaru Strait on the Japan Sea side, Japan; Tsingtao, China; Korea; and the Gulf of Tartary, Russia) (Hatai 1936a, 1936b, 1938; Logan 2007). *Laqueus rubellus* inhabits water depths of 44–907 m in the Pacific Ocean (the seas around Japan; the Japan Sea; Pailolo channel, Hawaii) (Dall 1920; Hatai 1936a; Logan 2007). The wide spatiotemporal distribution of these species means that their δ^{13}C and δ^{18}O values are potentially useful for reconstructing the paleoceanographic environments of lower sublittoral to upper bathyal zones during the late Mesozoic to Cenozoic.

Materials and sample sites
Modern specimens
Terebratalia coreanica from Otsuchi Bay

Modern *T. coreanica* (OTTCo; Fig. 1a) were collected by dredging at 70 m water depth in Otsuchi Bay (39° 21.86′ N, 141° 59.97′ E) along the Sanriku Ria Coast in northeastern Japan, using the research vessel *Yayoi* of the International Coastal Research Center, Atmosphere and Ocean Research Institute (ICRS/AORI), The University of Tokyo, on 12 September 2005. High-resolution, three-dimensional δ^{13}C and δ^{18}O values of this species have been published by Yamamoto et al. (2011, 2013). The δ^{13}C and δ^{18}O values of calcite precipitated in isotopic equilibrium with ambient seawater (equilibrium calcite) at the brachiopod collection site ranged from 1.4 to 2.6‰ (δ^{13}C$_{EC}$) and from – 1.4 to 2.4‰ (δ^{18}O$_{EC}$) (Yamamoto et al. 2011, 2013). The
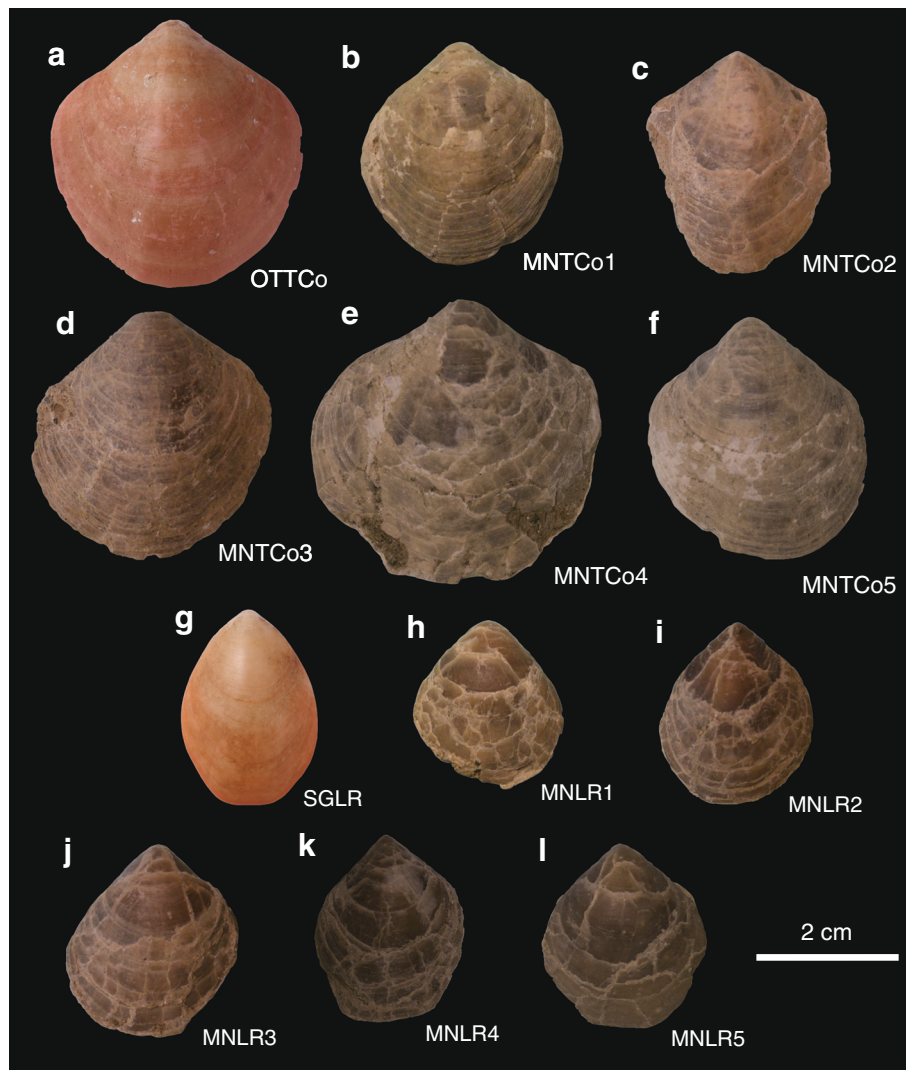
Fig. 1 Photographs of the *Terebratalia coreanica* and *Laqueus rubellus* shells examined in this study. The modern *T. coreanica* shells were collected from Otsuchi Bay, northeastern Japan, and *L. rubellus* shells were collected from Sagami Bay, central Japan. The fossil shells are from the Pliocene Tentokuji Formation in Minehama, northeastern Japan. **a** Modern *T. coreanica*. **b–f** Fossil *T. coreanica*. **g** Modern *L. rubellus*. **h–l** Fossil *L. rubellus*. Only the ventral valves were examined in this study

$\delta^{13}C_{EC}$ values were calculated by using the $\delta^{13}C$ values of inorganic carbon (DIC) at the brachiopod collection site (Otsuchi Bay), the difference between $\delta^{13}C_{HCO3-}$ and $^{13}C_{DIC}$ values (0.2‰, Grossman 1984, Romanek et al. 1992, Zhang et al. 1995), and the calcite-HCO_3^- enrichment factor (1.0 ± 0.20‰, Romanek et al. 1992) (Additional file 7: Doc. S1). The $\delta^{18}O_{EC}$ values were estimated based on the equation given by Friedman and O'Neil (1977) (Additional file 7: Doc. S1).
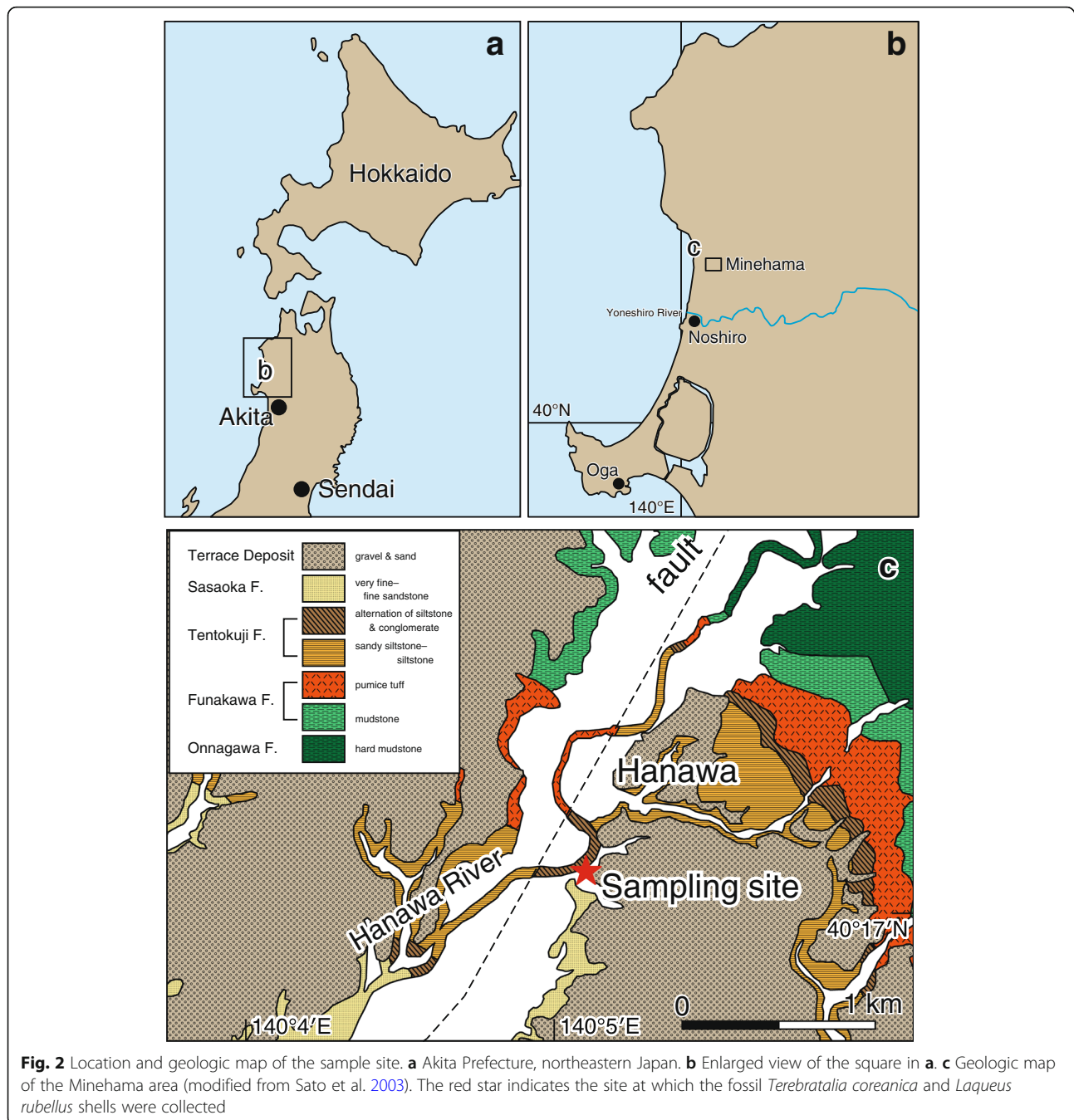
Laqueus rubellus from Sagami Bay

Modern *L. rubellus* (SGLR; Fig. 1g) were collected by dredging at 80 m water depth at the eastern margin of Sagami Bay, central Japan (35° 08.17′ N, 139° 34.86′ E), during a cruise of the fishing vessel *Rinkai-maru*, based

at the Misaki Marine Biological Station, The University of Tokyo, on 16 June 2005. Yamamoto et al. (2010a) have presented high-resolution, three-dimensional $\delta^{13}C$ and $\delta^{18}O$ values of this species. The $\delta^{13}C_{EC}$ values ranged from 1.6 to 2.6‰, and $\delta^{18}O_{EC}$ ranged from − 0.6 to 0.8‰ (Yamamoto et al. 2010a). These values were calculated by the same method as described above.

Fossil shells

Fossil *T. coreanica* (MNTCo1–MNTCo5; Fig. 1b–f) and *L. rubellus* (MNLR1–MNLR5; Fig. 1h–l) were collected from sandy conglomerates of the upper part of the Pliocene Tentokuji Formation exposed at Minehama (MH1, Amano et al. 2011), Happo-cho, Akita Prefecture, northeastern Japan (Fig. 2; 40° 17.18′ N, 140° 4.52′ E). The

Fig. 2 Location and geologic map of the sample site. **a** Akita Prefecture, northeastern Japan. **b** Enlarged view of the square in **a**. **c** Geologic map of the Minehama area (modified from Sato et al. 2003). The red star indicates the site at which the fossil *Terebratalia coreanica* and *Laqueus rubellus* shells were collected

horizon with the fossil brachiopod shells is dated 3.85–2.75 Ma, owing to its location between the Upper Pliocene datum planes (datum planes 21 and A) (Sato et al. 2003), which represent ages of 3.85 Ma and 2.75 Ma (Sato and Kameo 1996).

The Upper Miocene to Pleistocene succession around Minehama consists of the Onnagawa, Funakawa, Tentokuji, and Sasaoka formations in ascending order (Fig. 2c; Sato et al. 2003). The Onnagawa Formation is composed mainly of hard mudstone (generally termed "hard shale")

conformably overlain by the Funakawa Formation, which comprises mostly mudstone and pumice tuff. The Tentokuji Formation, conformably overlying the Funakawa Formation, consists mainly of dark bluish-gray siltstone alternating with conglomerates in the middle-upper intervals of the formation. The alternating beds are regarded as a turbidite sequence (Sato et al. 2003). The conglomerates yielding the brachiopod shells analyzed in the present study are 5–10 cm thick and consist of rounded to sub-rounded, granule to pebble-sized gravel

of andesite and, to a lesser extent, pumice, with a matrix of coarse-grained volcaniclastic sand. The Sasaoka Formation conformably overlies the Tentokuji Formation and consists of poorly sorted, very coarse to coarse-grained sandstone. Bivalves that co-occur with the brachiopods indicate a lower sublittoral zone depositional environment (Higo et al. 1999; Amano et al. 2011).
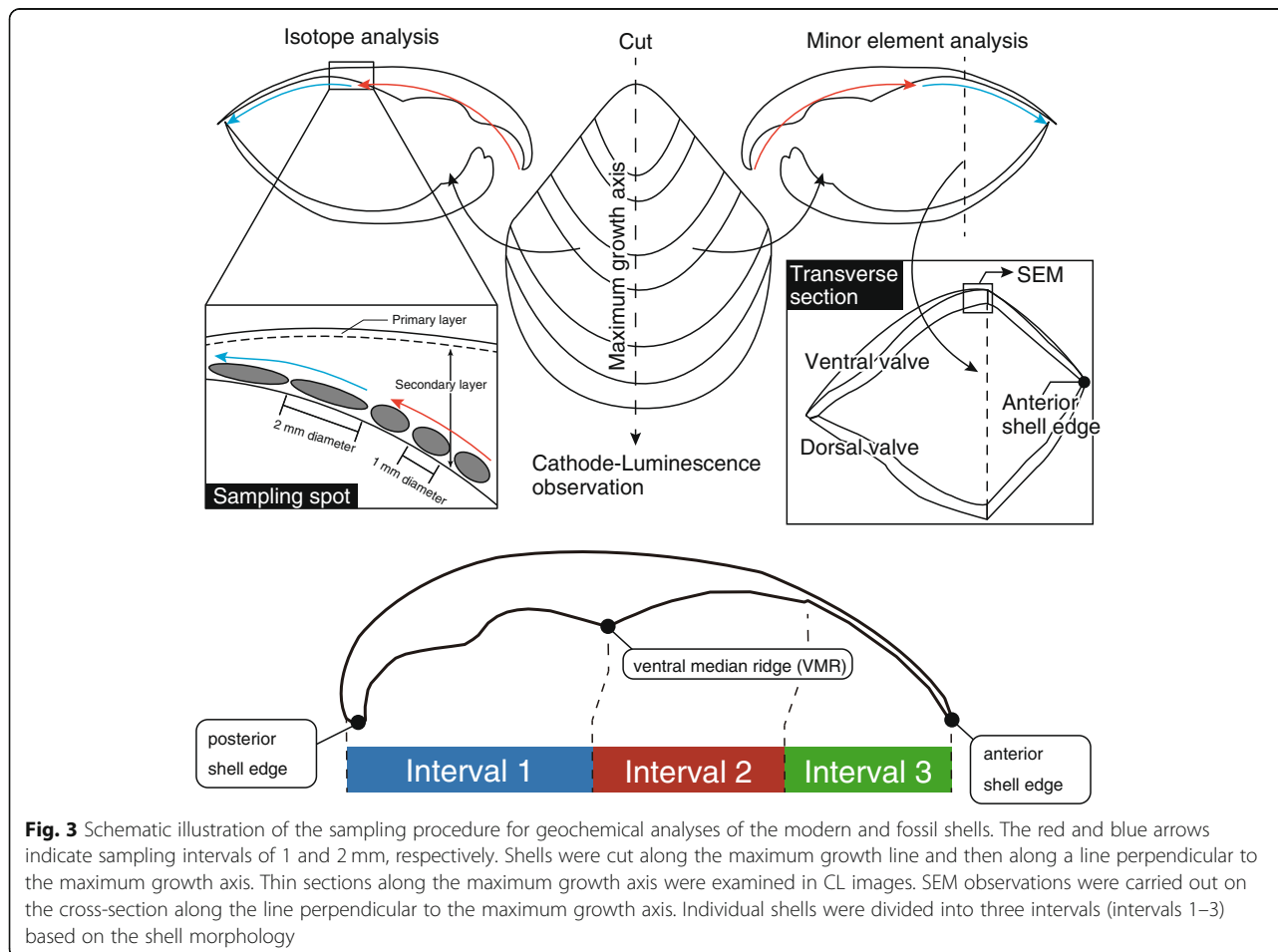
Methods/Experimental
High-resolution microsampling
The $\delta^{13}C$ and $\delta^{18}O$ values of the modern brachiopod shells display significant intra-shell, intra-species, and inter-species variations, and the isotope composition is not in all cases within the range of values of equilibrium calcite (Auclair et al. 2003; Yamamoto et al. 2010a, 2010b, 2011, 2013; Cusack et al. 2012; Takayanagi et al. 2012, 2013, 2015). Therefore, specific shell portions, for which the $\delta^{13}C$ and $\delta^{18}O$ values are identical to the $\delta^{13}C_{EC}$ and $\delta^{18}O_{EC}$ values, respectively, must be selected when using the isotopic signatures as paleoenvironmental proxies. Therefore, in recent studies, samples have been extracted from spot locations on the inner shell surfaces in vertical sections along the maximum growth (longitudinal) axis

(e.g., Angiolini et al. 2007; Garbelli et al. 2014, 2016; Takizawa et al. 2017). This procedure yields a relatively narrow range of $\delta^{13}C$ and $\delta^{18}O$ values because of the minimal fractionation effect in this region of the shell, arising from the very low growth (shell thickening) rate, except in and around specialized shell portions (e.g., muscle scars and the foramen).

Ventral valves of the brachiopod shells were embedded in a resin epoxy matrix and vertically cut along the maximum growth axis (Fig. 3) with a 0.4 mm thick IsoMet low-speed saw (Buehler, Lake Bluff). The samples for isotopic and minor element analyses (~ 0.1 mg for each analysis) were obtained from locations within 0.5 mm of the inner shell surface at 1 mm intervals (red arrows in Fig. 3) in a thick (> 1 mm) shell portion using a 0.2 mm diameter drill and at 2 mm intervals (blue arrows in Fig. 3) in a thin (< 1 mm) shell portion with a 0.10– 0.12 mm diameter drill. The sampled spots were ~ 0.6– 2.3 mm in length and less than 0.5 mm wide. We used a diamond-coated drill bit for extracting samples to prevent contamination by iron present in the drill bits.

Individual shells were divided into three intervals based on the shell morphology: interval 1 corresponding

Fig. 3 Schematic illustration of the sampling procedure for geochemical analyses of the modern and fossil shells. The red and blue arrows indicate sampling intervals of 1 and 2 mm, respectively. Shells were cut along the maximum growth line and then along a line perpendicular to the maximum growth axis. Thin sections along the maximum growth axis were examined in CL images. SEM observations were carried out on the cross-section along the line perpendicular to the maximum growth axis. Individual shells were divided into three intervals (intervals 1–3) based on the shell morphology

to a thick posterior shell region, interval 2 located between intervals 1 and 3, and interval 3 denoting the thin anterior shell region (Fig. 3). This division is identical to that proposed for *Kikaithyris hanzawai* shells (Takizawa et al. 2017). The boundary between intervals 1 and 2 in both species corresponded to a convex portion located in the center of ventral valves, which was identical to the "ventral median ridge (VMR)" reported from the ventral valves of *K. hanzawai* (Endo 1989), and hereafter, we use this term. The VMR was located 12.5–16.3 mm from the posterior shell edge in *T. coreanica* and 13.2–14.6 mm in *L. rubellus*. The boundary between intervals 2 and 3 was a region where the shell thickness became less than 1 mm. This region was located 4.6–12.8 and 3.8–10.2 mm from the VMR toward the anterior shell edge in *T. coreanica* shells and *L. rubellus* shells, respectively.

Powder samples were extracted from calcite cement in an internal cavity (7 mm × 4 mm in diameter) of a fossil brachiopod shell using the same method as described above. This brachiopod shell was small (a distance from the posterior shell edge to the anterior shell edge of < 1 cm) and was not used for geochemical analyses in this study. The inner shell surface of the fossil brachiopod was covered thinly with blocky equant calcites with undulated protuberances (~ 2 mm long and ~ 1 mm in diameter) showing a helictite-like appearance. This is the largest cement found in this study. Based on its location and morphology, this calcite cement is considered to have been formed by meteoric diagenesis. The intergranular space of the sandstone matrix was filled with submillimeter-sized, blocky cements. No sign of hydrothermal activity was found around the brachiopod sampling site (Minehama) or within the surrounding region.

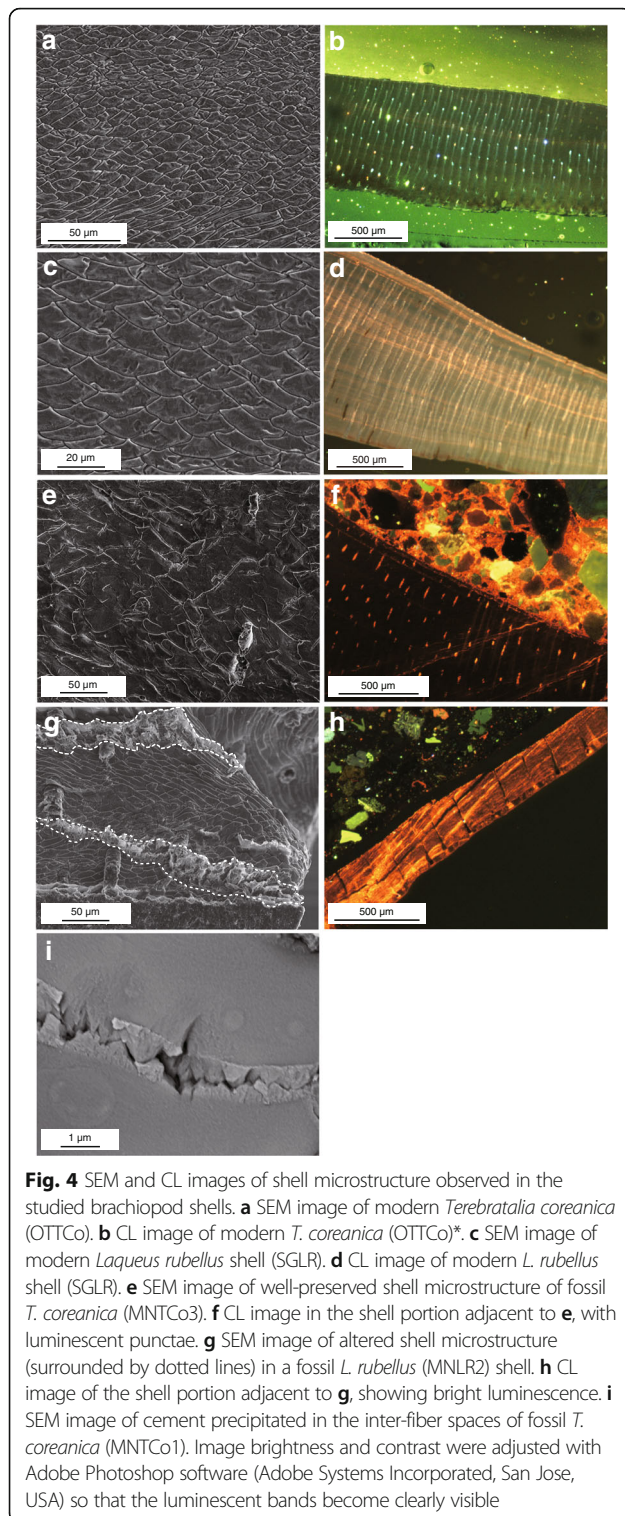## SEM, energy dispersive spectrometer (EDS), and CL observations

After the shells had been micro-sampled for isotopic and minor element analyses, they were cut parallel to the maximum growth axis and made into thin sections (Fig. 3). The spatial offset between the geochemical sampling and the CL sections were less than 0.5 mm. CL images of the thin sections were examined using a Relion Industries Reliotron VII cold cathodoluminescence microscope mounted on a polarizing microscope at the Department of Earth Sciences, Environmental and Resources Engineering, Waseda University, Japan. The beam current was ~ 0.06–0.2 mA, and the voltage was 10–13 kV. The beam diameters were ~ 7 mm for the observation of modern shells and ~ 1.5 cm for the fossil shells. We measured the mean CL intensity (MCLI) in the corresponding areas (~ 400 μm × 1000 μm and 200 μm × 2000 μm in thick and thin shell portions, respectively) of the isotopic and minor element sampling locations to quantify the degree of luminescence. The

CL images represent color information for each dot as a mixture of R (red), G (green), and B (blue), each represented in 256 gradations from 0 to 255. The MCLI was defined as the mean *R* values of a CL image. The *R* values were measured using ImageJ software developed at the National Institutes of Health, USA (ver. 1.59 m9 with Java 1.8.0_101).

After making the thin sections for CL observations, the shells were cut transversely (perpendicular to the maximum growth axis; Fig. 3) along a transect located ~ 13–35 mm from the posterior shell edge. The cut surface was etched with 0.2 mol/L hydrochloric acid (HCl) for 30 s and then coated with carbon. The surface was then observed using a Keyence VE-8800 SEM at the Institute of Geology and Paleontology, Graduate School of Science, Tohoku University (IGPS), with an accelerating voltage of 10 kV. The secondary shell layer of brachiopods is composed of calcite fibers that extend along the maximum growth axis. During diagenesis, these calcite fibers are dissolved and replaced with blocky calcite. The altered fibers become amalgamated, and their outlines become indistinct (Samtleben et al. 2001; Yamamoto et al. 2017). Traditionally, longitudinal sections are used to examine shell microstructure (e.g., Bates and Brand 1991; Qing and Veizer 1994; Azmy et al. 1998; Korte et al. 2005), but this diagenetic alteration of fibers can be observed more clearly in transverse sections, which enables a better determination to be made of whether or not the fibers retained their initial forms (e.g., Samtleben et al. 2001; Garbelli et al. 2014; Takizawa et al. 2017; Yamamoto et al. 2017).

Chemical microanalyses were performed using an Oxford Instruments energy dispersive spectrometer (EDS) installed in a JEOL JSM-7001F field emission SEM (FE-SEM) at the IGPS. The constant accelerating voltage for the EDS analysis was 15 kV and the probe current 1.47 A.

We compared the microstructures of the modern and fossil brachiopod shells and defined two divisions of preservation state: well-preserved (Fig. 4e, f) and diagenetically altered (Fig. 4g, h). In the well-preserved shell portions, the outlines of the calcite fibers were well defined, and each fiber was plainly discernible. In the altered portions, the individual fibers were unobservable owing to their amalgamation. We used two indices to quantify the preservation state of shell microstructure: altered fiber ratio (AFR) and altered fiber and puncta-filling cement ratio (AF-PCR). The former is defined as a ratio (%) of the area of altered fibers to the total area of fibers observed in a particular area (200 μm × 250 μm (magnification = × 400) or 212 μm × 266 μm (magnification = × 600)). The AF-PCR, which corresponds to the AFR of Yamamoto et al. (2017), represents a ratio (%) of the area occupied by altered fibers plus puncta-filling cement to the total area of the fibers where we measured

Fig. 4 SEM and CL images of shell microstructure observed in the studied brachiopod shells. **a** SEM image of modern *Terebratalia coreanica* (OTTCo). **b** CL image of modern *T. coreanica* (OTTCo)*. **c** SEM image of modern *Laqueus rubellus* shell (SGLR). **d** CL image of modern *L. rubellus* shell (SGLR). **e** SEM image of well-preserved shell microstructure of fossil *T. coreanica* (MNTCo3). **f** CL image in the shell portion adjacent to **e**, with luminescent punctae. **g** SEM image of altered shell microstructure (surrounded by dotted lines) in a fossil *L. rubellus* (MNLR2) shell. **h** CL image of the shell portion adjacent to **g**, showing bright luminescence. **i** SEM image of cement precipitated in the inter-fiber spaces of fossil *T. coreanica* (MNTCo1). Image brightness and contrast were adjusted with Adobe Photoshop software (Adobe Systems Incorporated, San Jose, USA) so that the luminescent bands become clearly visible

the AFR. We used the two indices because the impact of puncta-filling cement on the diagenetic modification of the isotopic compositions and minor element concentrations of the fossil shells is not negligible and needs to be properly evaluated. We did not measure these indices

for interval 1, as the isotopic compositions for this interval cannot be used for paleoenvironmental analysis, as discussed below.

Isotopic analysis

Stable carbon and oxygen isotope analyses of carbonate powder samples were performed using a Thermo Fisher Delta V Advantage isotope ratio mass spectrometer coupled to a ThermoQuest Kiel-III automated carbonate device, at the IGPS. The samples (~ 0.1 mg) were reacted with 100% phosphoric acid at $\sim 72\,°C$. The isotope ratios were expressed in conventional ($\delta\text{‰}$) notation and calibrated to the NBS-19 international standard relative to the Vienna Pee Dee Belemnite (VPDB). The external precision (1σ) based on replicate measurements ($n = 91$) of the laboratory reference material (JCt-1; Okai et al. 2004) was 0.02‰ for the carbon isotope analysis and 0.05‰ for oxygen isotope analysis.

It is known that the $\delta^{18}O$ values for magnesian calcite (Mg-calcite) are higher than those for pure calcite formed under the same conditions (e.g., Tarutani et al. 1969). However, if a fractionation correction for Mg-calcite relative to pure calcite (0.06‰ per mol% $MgCO_3$, according to Tarutani et al. 1969, 0.17‰ per mol% $MgCO_3$, according to Jiménez-López et al. 2004) is applied to $\delta^{18}O$ values of the studied shells, this effect is negligible or limited due to their low Mg contents ($<$ 1.18 mol% $MgCO_3$). Therefore, the Mg effect on the $\delta^{18}O$ values of brachiopod shells (Brand et al. 2013) does not need to be accounted for in this study.

Minor element analysis

Powdered brachiopod shell samples (20.5–189.8 μg) were dissolved in ~ 5.0–10.0 mL of volume-specific 2% (v/v) nitric acid (HNO_3). The volume of the acid was varied to adjust the Ca concentration in the solutions to ~ 3–4 ppm for most analyses. Concentrations of the three minor elements (Mn, Fe, and Sr) were analyzed using an Agilent 7700x inductively coupled plasma mass spectrometer at the Department of Earth and Environmental Sciences, Nagoya University, Japan. Minor elemental concentrations are expressed as ppm (= μg/g). The precision of the analytical method, expressed as the relative standard deviation (σ) of repeated analyses of the laboratory reference material (JCt-1; Okai et al. 2004), was 1.8–4.6% for Mn, 10.8–11.9% for Fe, and 2.2–2.4% for Sr.

Results

All analytical data are given in Additional file 1: Table S1, Additional file 2: Table S2, Additional file 3: Table S3, and Additional file 4: Table S4.

Fujioka *et al. Progress in Earth and Planetary Science* (2019) 6:45

Page 8 of 23

SEM, EDS, and CL observations
Modern shells

The shells of modern *T. coreanica* (OTTCo) and *L. rubellus* (SGLR) consisted of two calcite layers: the thinner outer primary shell layer and a thicker inner secondary shell layer (Fig. 4a, c). The primary shell layers of both brachiopod species displayed a fine granular structure measuring up to 30 μm thick in *T. coreanica* and up to 25 μm in *L. rubellus.* The secondary shell layer accounted for > 90% of the shell thickness and was composed of thin elongated calcite fibers oriented parallel or slightly oblique to the maximum shell growth axis. The two shell layers were penetrated with punctae perpendicular to the outer and inner shell surfaces. The calcite fibers within the secondary shell layer were clearly identifiable. We regarded this state as the initial fiber structure (Fig. 4a, c).

The modern shells of the two species exhibited intrinsic blue luminescence (Fig. 4b, d; Additional file 5: Figure S1-1b; Additional file 6: Figure S2–1b,) caused by a lack of Mn-activated visible luminescence and by crystal imperfections (Sippel and Glover 1965; Machel et al. 1991; Habermann et al. 1998). Here, we term this blue luminescence as "non-luminescence."

Fossil shells

The primary shell layer, which is commonly lost in fossil shells (Angiolini et al. 2007; Garbelli et al. 2014, 2017), was preserved in all fossil specimens (MNTCo1–MNTCo5 and MNLR1–MNLR5). The secondary shell layer of the fossil brachiopods consisted of calcite fibers (Fig. 4e) similar to those of the modern shells. However, traces of the dissolution and amalgamation of calcite fibers (Fig. 4g) were identified in many shell portions. The punctae (< 10 μm in diameter), perforations penetrating brachiopod shells, were scattered, commonly infilled with calcite cements. The abundance of altered structures was highly variable among the shell portions, with AFR values ranging from 0 to 92% and AF-PCR values from 1 to 95%.

Some parts of the fossil shells exhibited bright luminescence in CL images (Fig. 4f, h), with MCLI values ranging from 18 to 213 in *T. coreanica* and from 12 to 216 in *L. rubellus.* The strongly luminescent shell portions were also diagenetically altered, as indicated by the traces of dissolution and amalgamation of calcite fibers observed via SEM and the high AFR and AF-PCR values. The fossil shells had luminescent dots and lines (< 15 μm in diameter), each corresponding to a calcite cement filling a puncta (Fig. 5).

Submicron-sized, subhedral, blocky, isopachous fringing calcite cements were found in the inter-fiber spaces of some fossil brachiopod shells with SEM (Fig. 4i). These cements formed in a narrow space between the calcite fibers. The remnants of organic sheaths surrounding rarely

occurred. EDS analysis indicated that the Mn concentrations of these cements were as high as 22,000 ppm and their Fe concentrations up to 11,000 ppm, although the concentrations were highly variable. In contrast, Sr was not detected in such cements.

Isotopic composition
Modern shells

The $\delta^{13}C$ values of samples from the inner shell surfaces of modern *T. coreanica* from Otsuchi Bay (OTTCo) ranged from − 0.15 to 1.38‰ and from − 0.12 to 1.75‰ for $\delta^{18}O$ (Table 1, Fig. 6a, and Additional file 5: Figure S1-1). Interval 1 exhibited wider ranges of isotopic values than did intervals 2 and 3, containing two local $\delta^{13}C$ minima and four local $\delta^{18}O$ minima (Fig. 6a, and Additional file 5: Figure S1-1). The $\delta^{13}C$ profile in this interval consisted of lower values near the posterior shell edge and higher values near the VMR, which were separated by a local minimum $\delta^{13}C$ value between the two sections. The $\delta^{13}C$ values in the lower-value section varied within a narrow range of 0.16 to 0.51‰. In contrast, the $\delta^{13}C$ values in the higher-value section exhibited large-amplitude fluctuations within a range of − 0.15 to 1.38‰. The $\delta^{18}O$ profile exhibited large-amplitude fluctuations throughout interval 1. The $\delta^{13}C$ and $\delta^{18}O$ profiles in intervals 2 and 3 showed small-amplitude fluctuations with values from 0.65 to 1.36‰ for the $\delta^{13}C$ values and from 0.93 to 1.75‰ for the $\delta^{18}O$ values. Although the $\delta^{18}O$ values in intervals 1–3 were within the range of equilibrium calcite, the $\delta^{13}C$ values were not (Additional file 5: Figure S1-1).

The $\delta^{13}C$ and $\delta^{18}O$ values of samples from modern *L. rubellus* from Sagami Bay (SGLR) covaried ($r = 0.57$, $n = 27$, $p < 0.01$), ranging from 0.52 to 1.96‰ and from 0.26 to 0.94‰, respectively (Table 1, Fig. 6b, and Additional file 6: Figure S2-1). The $\delta^{13}C$ profile showed a gradual increase from 0.52 to 1.57‰ toward the VMR in interval 1, followed by a plateau ranging from 1.49 to 1.94‰ with an average value of 1.68‰ in interval 2 and a range of 1.28 to 1.96‰ (average 1.56‰) in interval 3 (Fig. 6b). The $\delta^{18}O$ values varied within a narrow range from 0.26 to 0.94‰ (average 0.62‰) throughout intervals 1–3. The $\delta^{18}O$ profile showed a gradually increasing trend in interval 1 and a decreasing trend in interval 3. The $\delta^{13}C$ values in interval 1 were lower than those of equilibrium calcite, and the $\delta^{13}C$ values in intervals 2 and 3 were slightly lower than or identical to the lowest values of equilibrium calcite (Additional file 6: Figure S2-1). The $\delta^{18}O$ values fell mostly in the upper half of the $\delta^{18}O$ range of equilibrium calcite.

Fossil shells

The $\delta^{13}C$ and $\delta^{18}O$ values of the five fossil *T. coreanica* (MNTCo1–MNTCo5) shells fell in wide ranges
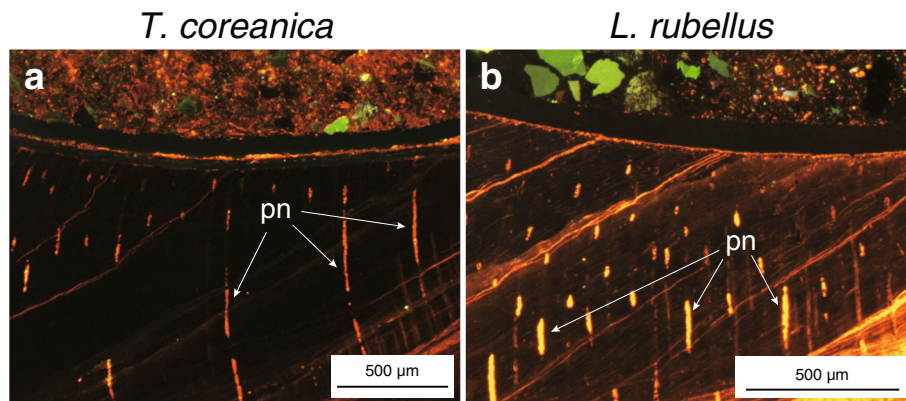
Fig. 5 CL images of puncta-filling cements. CL images of the vertical sections through the studied brachiopod shells (**a** *Terebratalia coreanica*, MNTCo2; **b** *Laqueus rubellus*, MNLR2). Note that strongly luminescent dots and lines each corresponding to a calcite cement filling a puncta

from − 3.31 to 2.43‰ for $\delta^{13}C$ and from − 0.42 to 2.18‰ for $\delta^{18}O$ (Table 1, Fig. 6a, and Additional file 5: Figures S1-2–6). The $\delta^{13}C$ profiles from interval 1 of the fossil shells had a wider range (2.41–4.37‰) than that of the modern shell (1.53‰). These $\delta^{13}C$ profiles for interval 1 generally followed the pattern of a lower-value section near the posterior shell edge and a higher-value section near the VMR. These two sections were separated by a local minimum $\delta^{13}C$ value, with an overall increasing trend toward the VMR. This was the same pattern seen in the modern shell. However, the higher-value section near the VMR of interval 1 from two shells (MNTCo2 and MNTCo5; Additional file 5: Figure S1-3, 6) was associated with a local minimum in $\delta^{13}C$ values. The $\delta^{13}C$ profiles from intervals 2 and 3 of the fossil shells exhibited a different trend from the same intervals of the modern shell. Shells MNTCo1 and MNTCo2 both showed a high-value plateau extending over interval 2. The $\delta^{13}C$ profile of MNTCo3 was similar to those of MNTCo1 and MNTCo2 but exhibited a local minimum in this interval (Additional file 5: Figures S1-2–4). Interval 2 of shells MNTCo4 and MNTCo5 exhibited a short high-value plateau near the VMR, followed by a marked decrease toward the anterior shell edge. The $\delta^{13}C$ values in interval 3 were lower than those of the high-value plateau in interval 2. Shell MNTCo1 had a local $\delta^{13}C$ minimum in this interval, and shell MNTCo3 had two local minima (Additional file 5: Figures S1-2, 4).

$\delta^{18}O$ profiles of intervals 1 and 2 of the fossil *T. corea-nica* were similar to those of the modern shell. Interval 1 had larger $\delta^{18}O$ amplitudes than did intervals 2 and 3 as a result of a series of erratic, negative $\delta^{18}O$ spikes. The $\delta^{18}O$ values were more consistent in interval 2 than in intervals 1 and 3. Each profile from interval 2 fell in a narrow range (0.07–1.22‰), and the total range of the

$\delta^{18}O$ values from the five shells was only 1.44‰. The $\delta^{18}O$ values in interval 3 of the three fossil shells (MNTCo2, MNTCo4, and MNTCo5) fell in a narrow range (0.28–0.57‰), as did the modern shell (0.82‰). The other two fossil shells (MNTCo1 and MNTCo3) exhibited distinct negative spikes in the $\delta^{18}O$ profiles in interval 3 (one in MNTCo1 and two in MNTCo3; Additional file 5: Figure S1-2, 4).

The $\delta^{13}C$ values of samples from fossil *L. rubellus* shells (MNLR1–MNLR5) ranged from − 3.58 to 2.42‰, and $\delta^{18}O$ ranged from 0.03 to 2.37‰ (Table 1, Fig. 6b, and Additional file 6: Figures S2-2–6). The $\delta^{13}C$ values in interval 1 were highly variable, and each profile had a wider range (3.07–5.47‰, average 3.71‰) compared with the modern shell (1.05‰, Fig. 6b). The gradually increasing trend in $\delta^{13}C$ toward the VMR in this interval was recognized in the fossil shells, but it was not as obvious as in the modern shell. The $\delta^{13}C$ profiles showed three trends in interval 2: relatively constant (MNLR1 and MNLR3), increasing toward the anterior (MNLR4), and decreasing toward the anterior (MNLR2 and MNLR5). The $\delta^{13}C$ values were again highly variable in interval 3 without any common trend among the fossil shells, and almost all values were lower than those of the modern shell except for one (MNLR1).

The $\delta^{18}O$ values of fossil *L. rubellus* shells were less varied than the $\delta^{13}C$ values throughout the three intervals. Each profile exhibited a narrow range (1.23–1.81‰), and the total range of the $\delta^{18}O$ values from the five shells was < 2.34‰.

Calcite cement
The $\delta^{13}C$ and $\delta^{18}O$ values of the calcite cement sample were much lower than those of the fossil shells. The mean values from eight repeated measurements were − 17.87‰ ($\sigma = 0.12$‰) for $\delta^{13}C$ and − 6.62‰ ($\sigma = 0.09$‰) for $\delta^{18}O$ (Fig. 7).

Table 1 Modern and fossil *Terebratalia coreanica* and *Laqueus rubellus* δ^{13}C and δ^{18}O values and minor-element concentrations

Sample No.	Interval 1			Interval 2			Interval 3		
	Range	Average	Median	Range	Average	Median	Range	Average	Median
T. coreanica									
δ^{13}C (‰ VPDB)									
OTTCo	− 0.15 to 1.38	0.56	0.45	1.01 to 1.36	1.19	1.19	0.65 to 1.17	1.03	1.05
MNTCo1	−2.02 to 1.69	−0.43	−0.46	2.10 to 2.40	2.19	2.13	−2.98 to 1.70	0.31	0.84
MNTCo2	−2.30 to 1.30	−0.64	− 0.93	1.17 to 2.15	1.81	1.96	0.06 to 0.65	0.34	0.28
MNTCo3	−2.78 to 1.59	−0.05	− 0.07	0.59 to 1.98	1.57	1.73	−3.31 to 0.46	−1.16	−0.94
MNTCo4	−1.76 to 0.65	− 0.25	− 0.25	− 0.03 to 2.43	1.21	1.01	−0.10 to 0.54	0.22	0.22
MNTCo5	−1.89 to 2.08	0.16	0.00	−0.01 to 2.14	1.23	1.22	0.27 to 1.19	0.77	0.82
δ^{18}O (‰ VPDB)									
OTTCo	−0.12 to 1.75	1.04	1.12	1.17 to 1.43	1.36	1.41	0.93 to 1.75	1.39	1.47
MNTCo1	−0.42 to 2.18	1.18	1.35	2.06 to 2.13	2.08	2.07	−0.21 to 2.00	1.34	1.76
MNTCo2	0.51 to 1.42	1.00	1.07	0.98 to 1.48	1.29	1.35	0.97 to 1.54	1.20	1.18
MNTCo3	0.50 to 1.62	1.11	1.22	0.93 to 1.64	1.37	1.35	0.10 to 1.36	0.70	0.75
MNTCo4	−0.26 to 1.60	0.70	0.60	0.69 to 1.91	1.55	1.63	1.06 to 1.53	1.31	1.32
MNTCo5	0.41 to 1.83	1.33	1.38	0.99 to 1.97	1.57	1.67	1.33 to 1.61	1.51	1.55
Mn (ppm)									
OTTCo	2 to 10	5	4	3 to 7	4	3	2 to 8	5	5
MNTCo1	80 to 2000	480	240	90 to 260	160	130	380 to 3000	1200	1100
MNTCo2	270 to 1900	770	700	390 to 3300	1100	420	580 to 2300	1600	1700
MNTCo3	170 to 1800	450	240	290 to 1300	530	390	1600 to 2500	1900	1700
MNTCo4	150 to 440	250	250	180 to 1700	700	570	790 to 1400	1100	1100
MNTCo5	150 to 1000	450	400	230 to 2700	910	770	600 to 1600	1000	890
Fe (ppm)									
OTTCo	30 to 1100	250	110	50 to 800	250	70	50 to 360	150	70
MNTCo1	590 to 5800	1800	1200	1200 to 1900	1500	1300	2000 to 6900	3900	2900
MNTCo2	200 to 2000	680	530	240 to 2400	870	400	860 to 3600	1800	1500
MNTCo3	200 to 4400	1300	770	220 to 970	470	400	1200 to 3200	2000	1500
MNTCo4	310 to 1500	670	580	870 to 3300	2000	1900	3800 to 4200	4000	4000
MNTCo5	1400 to 4900	2600	2100	1100 to 4700	2300	2000	2200 to 4200	3200	3400
Sr (ppm)									
OTTCo	810 to 1100	980	960	880 to 1000	960	960	890 to 1000	970	980
MNTCo1	820 to 1000	910	920	860 to 950	910	920	810 to 960	910	910
MNTCo2	730 to 950	850	850	840 to 940	890	890	850 to 920	890	880
MNTCo3	790 to 1000	900	910	820 to 920	870	870	810 to 870	830	830
MNTCo4	890 to 1100	980	970	780 to 990	880	870	830 to 940	890	890
MNTCo5	790 to 1000	890	880	820 to 910	860	860	850 to 880	860	860
L. rubellus									
δ^{13}C (‰ VPDB)									
SGLR	0.52 to 1.57	1.06	1.09	1.49 to 1.94	1.68	1.68	1.28 to 1.96	1.56	1.59
MNLR1	−0.97 to 2.12	0.80	1.07	1.89 to 2.39	2.07	1.93	–	–	–
MNLR2	−1.41 to 1.74	0.21	0.33	−0.26 to 1.86	1.02	1.46	−1.51 to 0.57	−0.52	−0.41
MNLR3	−3.58 to 1.89	−0.57	−0.32	1.94 to 2.42	2.21	2.27	0.45 to 1.23	0.73	0.64
MNLR4	−2.65 to 0.42	−1.32	−1.50	−0.23 to 1.87	0.85	0.84	−2.82 to 0.58	−1.24	−1.49
MNLR5	−1.69 to 2.06	0.69	0.33	−1.15 to 2.23	1.10	1.60	−1.87 to 1.07	−0.21	0.18

Table 1 Modern and fossil *Terebratalia coreanica* and *Laqueus rubellus* δ^{13}C and δ^{18}O values and minor-element concentrations *(Continued)*

Sample No.	Interval 1			Interval 2			Interval 3		
	Range	Average	Median	Range	Average	Median	Range	Average	Median
δ^{18}O (‰ VPDB)									
SGLR	0.26 to 0.94	0.60	0.61	0.55 to 0.93	0.74	0.73	0.26 to 0.81	0.53	0.43
MNLR1	1.14 to 2.09	1.67	1.71	2.09 to 2.33	2.19	2.17	–	–	–
MNLR2	0.74 to 1.79	1.16	1.16	0.91 to 1.96	1.53	1.73	0.24 to 1.44	0.73	0.66
MNLR3	0.03 to 1.50	0.88	1.04	1.54 to 1.85	1.69	1.68	0.96 to 1.57	1.15	0.98
MNLR4	0.29 to 1.31	0.83	0.86	1.19 to 2.00	1.59	1.55	0.53 to 1.66	1.01	0.83
MNLR5	0.63 to 1.92	1.34	1.42	0.56 to 2.12	1.61	2.00	0.31 to 1.44	0.95	1.10
Mn (ppm)									
SGLR	4 to 20	9	7	6 to 10	8	7	10 to 30	20	10
MNLR1	150 to 760	370	310	260 to 500	380	370	–	–	–
MNLR2	170 to 1100	620	650	180 to 1200	610	530	450 to 2000	1300	1300
MNLR3	130 to 2700	1100	680	170 to 260	210	200	800 to 2100	1300	1200
MNLR4	490 to 1900	1100	930	260 to 700	380	280	410 to 1700	1200	1300
MNLR5	160 to 940	410	340	120 to 1900	710	240	760 to 1000	900	920
Fe (ppm)									
SGLR	70 to 10,100	1300	620	70 to 1200	310	120	100 to 3600	1100	510
MNLR1	410 to 3900	1000	640	1200 to 3200	2000	1600	–	–	–
MNLR2	180 to 5000	1100	400	230 to 750	500	500	1300 to 5800	3200	2800
MNLR3	340 to 2700	1200	1200	440 to 4900	1900	510	2000 to 4200	2800	2600
MNLR4	600 to 1500	1100	1000	400 to 940	640	610	900 to 3400	2500	2900
MNLR5	510 to 3100	1300	1000	830 to 4700	2000	1600	2700 to 5100	3500	3200
Sr (ppm)									
SGLR	860 to 1100	990	1000	800 to 860	830	820	870 to 980	920	930
MNLR1	930 to 1000	980	970	880 to 920	900	900	–	–	–
MNLR2	850 to 1000	920	930	830 to 890	860	850	820 to 970	890	880
MNLR3	730 to 1000	870	890	850 to 860	850	850	810 to 1000	890	890
MNLR4	800 to 880	840	830	830 to 870	850	850	730 to 940	820	800
MNLR5	870 to 970	920	920	800 to 890	840	830	900 to 1000	950	950

Minor elements

Modern shells

The minor element concentrations ($n = 30$) in the modern *T. coreanica* shell fell within the ranges of 2–10 ppm (mean = 5 ppm, σ = 3 ppm, median = 4 ppm) for Mn, 30–1100 ppm (mean = 220 ppm, σ = 260 ppm, median = 100 ppm) for Fe, and 810–1100 ppm (mean = 980 ppm, σ = 80 ppm, median = 980 ppm) for Sr (Table 1, Fig. 6a, and Additional file 5: Figure S1-1). The profiles of these elements showed no systematic variations.
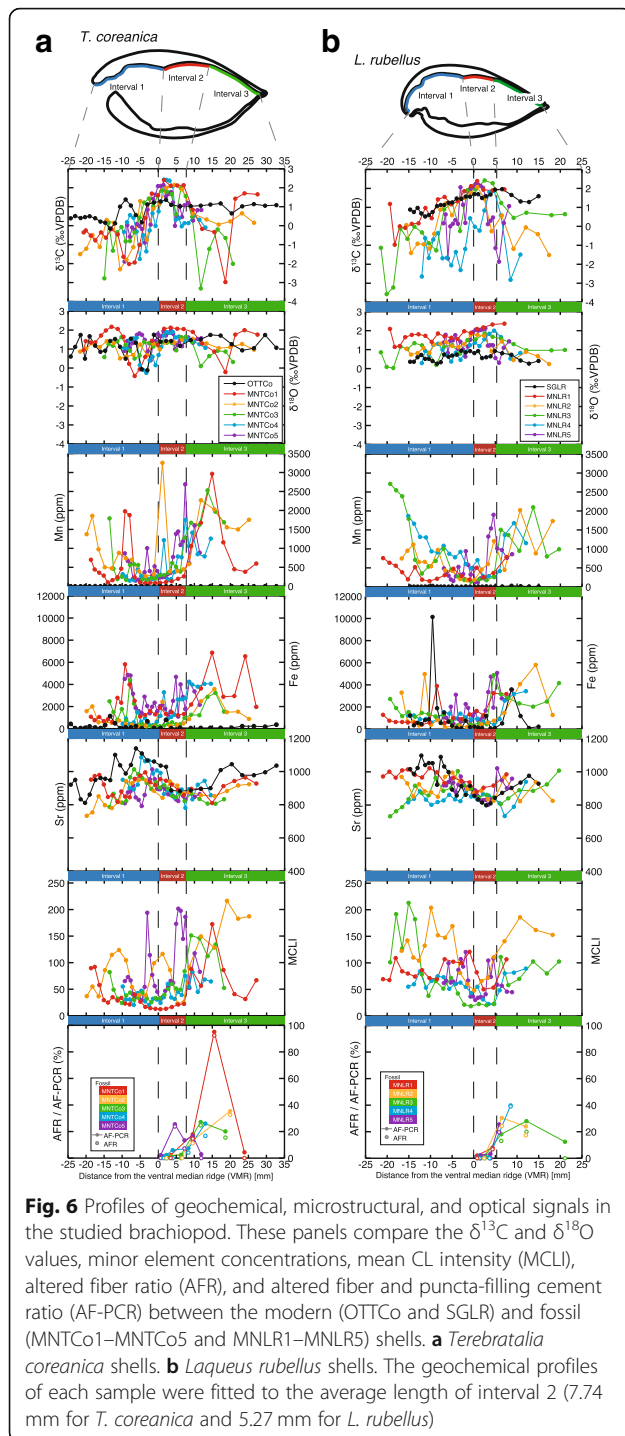
In the modern *L. rubellus* shell, minor element concentrations ($n = 27$) ranged from 4 to 30 ppm (mean = 10 ppm, σ = 6 ppm, median = 8 ppm) for Mn, 70 to 10,100 ppm (mean = 1000 ppm, σ = 2000 ppm, median = 510 ppm) for Fe, and 800–1100 ppm (mean = 940 ppm, σ = 90 ppm, median = 920 ppm) for Sr

(Table 1, Fig. 6b, and Additional file 6: Figure S2-1) and also showed no systematic variations.

Fossil shells

The minor element concentrations ($n = 127$) in the fossil *T. coreanica* (MNTCo1–MNTCo5) shells varied between 80 and 3300 ppm (mean = 580–1100 ppm, σ = 470–800 ppm, median = 280–740 ppm) for Mn, 200 and 6900 ppm (mean = 1000–2600 ppm, σ = 930–1700 ppm, median = 600–2200 ppm) for Fe, and 730 and 1100 ppm (mean = 870–930 ppm, σ = 50–80 ppm, median = 860–920 ppm) for Sr (Table 1, Fig. 6a, and Additional file 5: Figures S1-2–6).

In the fossil *L. rubellus* shells, minor element concentrations ($n = 103$) of (MNLR1–MNLR5) fell in the ranges of

Fig. 6 Profiles of geochemical, microstructural, and optical signals in the studied brachiopod. These panels compare the $\delta^{13}C$ and $\delta^{18}O$ values, minor element concentrations, mean CL intensity (MCLI), altered fiber ratio (AFR), and altered fiber and puncta-filling cement ratio (AF-PCR) between the modern (OTTCo and SGLR) and fossil (MNTCo1–MNTCo5 and MNLR1–MNLR5) shells. **a** *Terebratalia coreanica* shells. **b** *Laqueus rubellus* shells. The geochemical profiles of each sample were fitted to the average length of interval 2 (7.74 mm for *T. coreanica* and 5.27 mm for *L. rubellus*)

120–2700 ppm (mean = 400–1000 ppm, σ = 200–830 ppm, median = 370–910 ppm) for Mn, 180–5800 ppm (mean = 1300–1900 ppm, σ = 830–1800 ppm, median = 670–1500 ppm) for Fe, and 730–1000 ppm (mean = 840–960 ppm, σ = 40–70 ppm, median = 830–970 ppm) for Sr (Table 1, Fig. 6b, and Additional file 6: Figures S2-2–6).

Roughly speaking, the Mn and Fe concentrations in the fossil shells of both species decreased from the

posterior shell edge toward the VMR and increased toward the anterior shell edge. In contrast, the Sr concentrations in the fossil shells (*T. coreanica*, 730–1100 ppm; *L. rubellus*, 730–1000 ppm) were comparable with those of the modern shells (*T. coreanica*, 810–1100 ppm; *L. rubellus*, 800–1100 ppm). As with the modern shells, no discernable patterns were seen in the Sr profiles.

Calcite cement

The minor element concentrations of the calcite cement sample were 6200 ppm for Mn, 14,400 ppm for Fe, and 440 ppm for Sr. Mn concentration was 6 times higher than the median concentrations of the fossil shells, and the Fe concentration was 7 times higher. The Sr concentration of the cement was lower than that of the fossil shells.

Discussion

The diagenetic modification of isotope compositions

The $\delta^{13}C$ and $\delta^{18}O$ profiles in interval 1 of the modern *T. coreanica* shell are characterized by the occurrence of two local $\delta^{13}C$ minima and four local $\delta^{18}O$ minima. Similar depletions are found in the same interval of the modern *L. rubellus* shell, although they are not so distinct as those in the *T. coreanica* shell. Interval 1 includes the region of the shell to which the diductor and adjustor muscles are attached (Shiino and Kitazawa 2010) and a shell cavity where the digestive and reproductive organs are housed (Williams and Rowell 1965). This suggests that the observed $\delta^{18}O$ minima are potentially related to the biological activities of the brachiopods, although we cannot specify the exact mechanism. The $\delta^{13}C$ values of the muscle scar are up to 2‰ lower than those of the secondary shell layer (Parkinson et al. 2005; Yamamoto et al. 2010a, 2013) due to secondary calcification, which has been reported in the muscle scars, loop, and teeth (Williams 1968). Therefore, it is highly likely that the depletion of the $\delta^{13}C$ values in interval 1 is caused by precipitation and/or dissolution (Hughes et al. 1988) around the specialized portions.

The $\delta^{13}C$ amplitude in intervals 2 and 3 of the fossil brachiopods is ∼ 7.0–7.5 times greater than those of modern shells, and the $\delta^{18}O$ amplitude is ∼ 3 times greater. The $\delta^{13}C$ and $\delta^{18}O$ values of these intervals in three *T. coreanica* and four *L. rubellus* shells display significant positive correlations (*T. coreanica*: r = 0.89–0.98, p < 0.01, excluding MNTCo2 and MNTCo4; *L. rubellus*: r = 0.88–0.99, p < 0.01, excluding MNLR1) (Fig. 7). Both $\delta^{13}C$ and $\delta^{18}O$ trend negatively toward the $\delta^{13}C$ and $\delta^{18}O$ values of the calcite cement. The $\delta^{18}O$ value of calcite precipitated in oxygen isotope equilibrium with meteoric water in northeastern Japan, including the Minehama region ($\delta^{18}O$ of meteoric water = − 7.7 to − 10‰ VSMOW; Mizota and Kusakabe 1994) at the mean

Fig. 7 Cross-plots of δ¹³C versus δ¹⁸O values of the studied brachiopod shells. The samples were extracted from the modern and fossil *T. coreanica* and *L. rubellus* shells. The cement δ¹³C versus δ¹⁸O values are also plotted
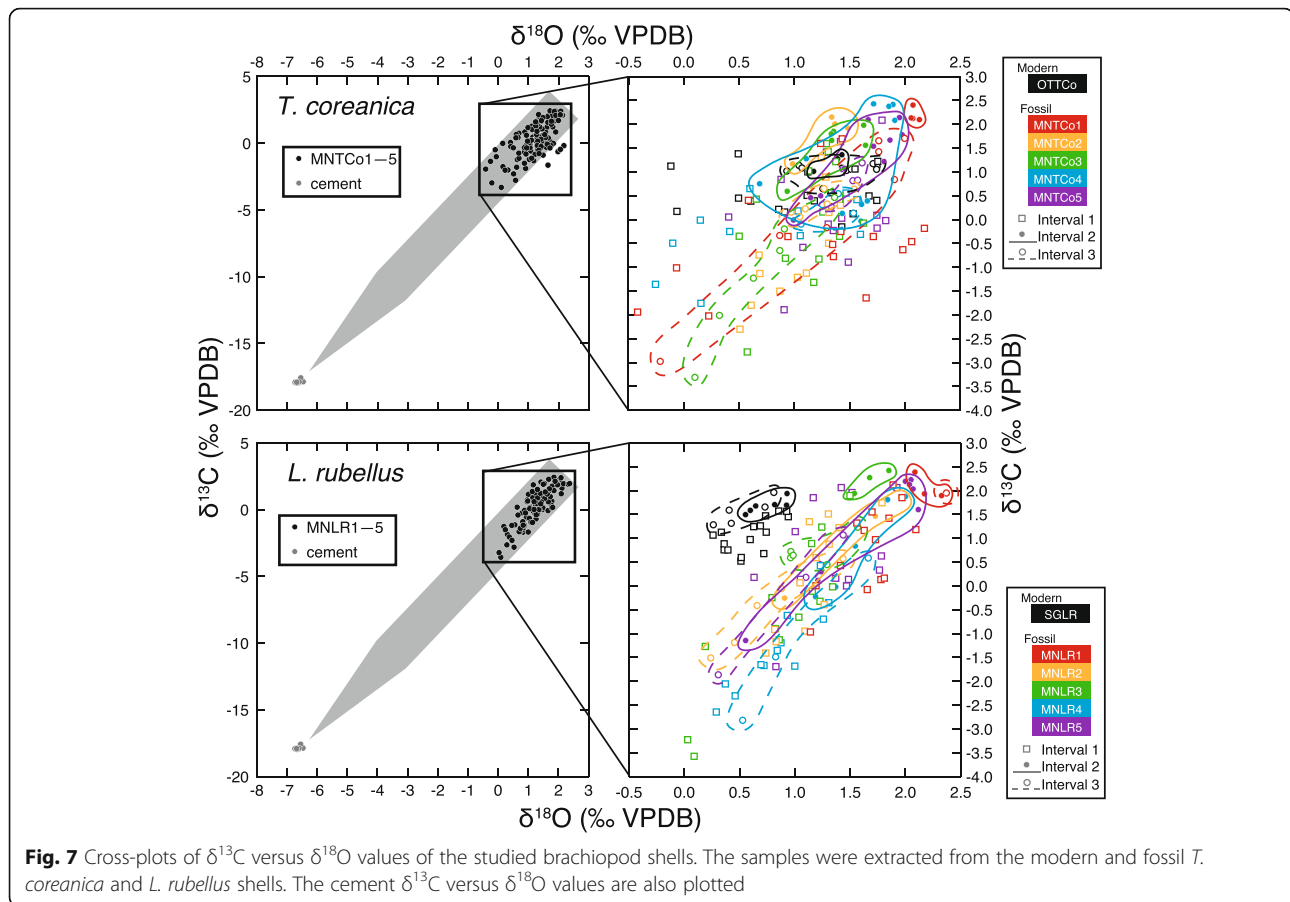
annual temperature (11.2 °C, Japan Meteorological Agency 2018) is estimated to be − 6.62 to − 8.92‰ following Friedman and O'Neil (1977). The δ¹⁸O of the calcite cement (− 6.62‰) falls within this range, indicating that the δ¹³C and δ¹⁸O values of the highest end-members on the cross-plots are close to their initial values and that the isotopic values of brachiopod shells at Minehama decreased toward those of the cement during meteoric diagenesis.

Another explanation for the positive correlation of the δ¹³C and δ¹⁸O values is a kinetic isotopic fractionation effect. Kinetic isotope fractionation during CO_2 hydration and hydroxylation results in an enhanced incorporation of ¹²C and ¹⁶O during precipitation of skeletal carbonates (McConnaughey 1989a, 1989b; McConnaughey et al. 1997; Auclair et al. 2003; Yamamoto et al. 2013; Takayanagi et al. 2015). This effect is closely related to rapid growth rates and high metabolic activity and is typically characterized by a positive correlation between δ¹³C and δ¹⁸O values (or $δ^{13}C–δ^{13}C_{EC}$ and $δ^{18}O–δ^{18}O_{EC}$ values). However, it is reported that growth rates along the inner surface (i.e., shell thickening rates) of brachiopod shells, including *T. coreanica* and *L. rubellus*, are very slow and that within a single

shell, the kinetic effect is negligible there (Yamamoto et al. 2010b, 2013). The δ¹³C and δ¹⁸O values of interval 1 are less strongly correlated than those of intervals 2 and 3 (Fig. 7). This is because the isotopic composition in interval 1 of the fossil shells is influenced by the biogenic effect mentioned above as well as by meteoric diagenetic modification.

The isotopic data indicate that the highest end-members on the cross-plots (Fig. 7) are likely to be closest to the initial shell δ¹³C and δ¹⁸O values. The highest end-members are from samples extracted from the thick portion of interval 2. This portion corresponds to "interval 2" of Pleistocene *K. hanzawai* shells from the Ryukyu Islands (Takizawa et al. 2017), which was regarded as a good shell portion to use for paleoenvironmental reconstructions because it exhibited relatively small intra-shell and intra-species variations. Therefore, this interval is likely to be a good region of the shells for paleoenvironmental analysis in many brachiopod taxa.

The diagenetic modification of minor element concentrations

Minor element concentrations in carbonate minerals have been used to identify diagenetically altered

brachiopod shells or shell portions (e.g., Wenzel 2000; Ullmann et al. 2014). As meteoric water generally contains more Mn and Fe and less Sr compared with seawater, Fe and Mn concentrations increase and Sr concentration decreases in diagenetically altered marine carbonates (Brand and Veizer 1980; Marshall 1992).

The Mn concentrations in the studied modern shells are relatively uniform. Concentrations in *T. coreanica* fall within a narrow range of 2–12 ppm, and *L. rubellus* concentrations are between 4 and 30 ppm (Fig. 6a, b). These ranges are comparable with values reported in previous studies of modern brachiopod shells (5–500 ppm, Morrison and Brand 1986; 0–200 ppm, Brand et al. 2003; 4–30 ppm, Lee et al. 2004; 0–70 ppm, Ullmann et al. 2017) and are lower than the common Mn concentrations in modern shells (< 80 ppm) compiled by Brand et al. (2003).

In contrast, the Mn concentration in the fossil *T. coreanica* and *L. rubellus* shells is higher than that of the modern shells. The observed range is 80–3300 ppm in the *T. coreanica* shells and is 120–2700 ppm in the *L. rubellus* shells. These values exceed the common Mn concentration in modern shells (Brand et al. 2003) and indicate that there are significant intra-shell and intra-species variations in the fossil brachiopod Mn concentrations (Fig. 6). The samples with high Mn concentrations did not correspond to specific regions of the shells but exhibited low $\delta^{13}C$ and $\delta^{18}O$ values, high Fe concentrations, and strong luminescence (Fig. 6, Additional file 5: Figures S1-2–6, and Additional file 6: Figures S2-2–6). This indicates that the increased Mn concentrations are the result of meteoric diagenetic alteration.

Although some anomalously high Fe concentrations (> 600 ppm) are observed, the range of Fe concentrations in the modern *T. coreanica* shells ranged from 30 and 490 ppm and from 70 to 570 ppm in *L. rubellus* (Fig. 6a, b). These values exceed the common Fe concentrations of modern brachiopod shells (< 140 ppm) presented by Brand et al. (2003). This difference is at least partly due to the fact that the Fe concentration threshold reported in Brand et al. (2003) was derived from bulk shell samples, which represent spatially averaged values.

The Fe concentrations in the fossil *T. coreanica* (200 to 6900 ppm) and *L. rubellus* (180 to 5800 ppm) shells are much higher than those of the modern shells and the common Fe concentration range (Brand et al. 2003). The samples with high Fe concentrations also exhibited high Mn concentrations, low $\delta^{13}C$ and $\delta^{18}O$ values, and strong luminescence. As with Mn, anomalously high Fe concentrations also occur in the fossil shells. These anomalously high concentrations are not always associated with any microstructural (dissolution and amalgamation of fibers), optical (strong luminescence on CL images; see below), or geochemical (decreased $\delta^{13}C$ or $\delta^{18}O$ values or increased Mn concentration) signals of diagenetic alteration. As

such, we consider that these anomalously high Fe concentrations are likely not diagenetic products but represent initial concentrations from when the brachiopods were alive. Similar anomalously high Fe concentrations without signs of diagenetic alteration in well-preserved fossil (~ 20 and ~ 70 ka) *K. hanzawai* shells have also been described by Takizawa et al. (2017).

Unlike Mn and Fe concentrations, Sr concentrations in the modern and fossil brachiopod shells were similar and their ranges overlap (Table 1). This indicates that Sr concentration in these brachiopod shells is not likely to be a good indicator of diagenetic alteration. The Mn and Sr concentrations show a moderate negative correlation (fossil *T. coreanica*: $r = - 0.46$, $p < 0.01$, Fig. 8c; fossil *L. rubellus*: $r = - 0.52$, $p < 0.01$, Fig. 8d). This differs from the result of Jelby et al. (2014), who found that Mn/Ca of diagenetically altered Lower Maastrichtian brachiopod shells was strongly negatively correlated with Sr/Ca ($r = - 0.94$).

The Mn concentrations in the calcite cement were ~ 2–3 times higher than the maximum Mn concentrations in the fossil shells, and Fe concentrations were ~ 2 times higher. This indicates that Mn and Fe concentrations in brachiopod shells at Minehama increased during meteoric diagenesis, approaching those of the cement. The Sr concentrations in the calcite cements were ~ 50% or less of mean Sr concentrations in the fossil shells. This implies that Sr concentrations in brachiopod shells at Minehama decreased during meteoric diagenesis, approaching those of the cement. However, the decrease in the Sr concentrations was relatively more gradual than the increase in the Mn and Fe concentrations. This is the reason why Sr is not sensitive to diagenesis at Minehama and shows a moderate negative correlation with the Mn concentrations. In conclusion, our study shows that of the three minor elements analyzed in this study, Mn concentration is the most reliable indicator of diagenetically altered shells or shell portions.

Diagenetic alteration detected by CL image observations

Cathodoluminescence observations are useful for determining the paragenetic sequences of diagenetic products precipitated from the solutions containing Mn. Altered shell portions are easily detectable by luminescence activated by the presence of Mn. It has been shown that the $\delta^{13}C$ and $\delta^{18}O$ values of luminescent shell portions are commonly lower than those of non-luminescent portions (e.g., Grossman et al. 1993; Mii et al. 2012).

The modern *T. coreanica* and *L. rubellus* shells exhibit faint to weak luminescent bands that are arranged almost parallel to the inner shell surface (Fig. 4b, d; Additional file 5: Figure S1-1b, and Additional file 6: Figure S2-1b). Similar luminescent bands are observed in shells of modern inarticulate brachiopods and in those of other
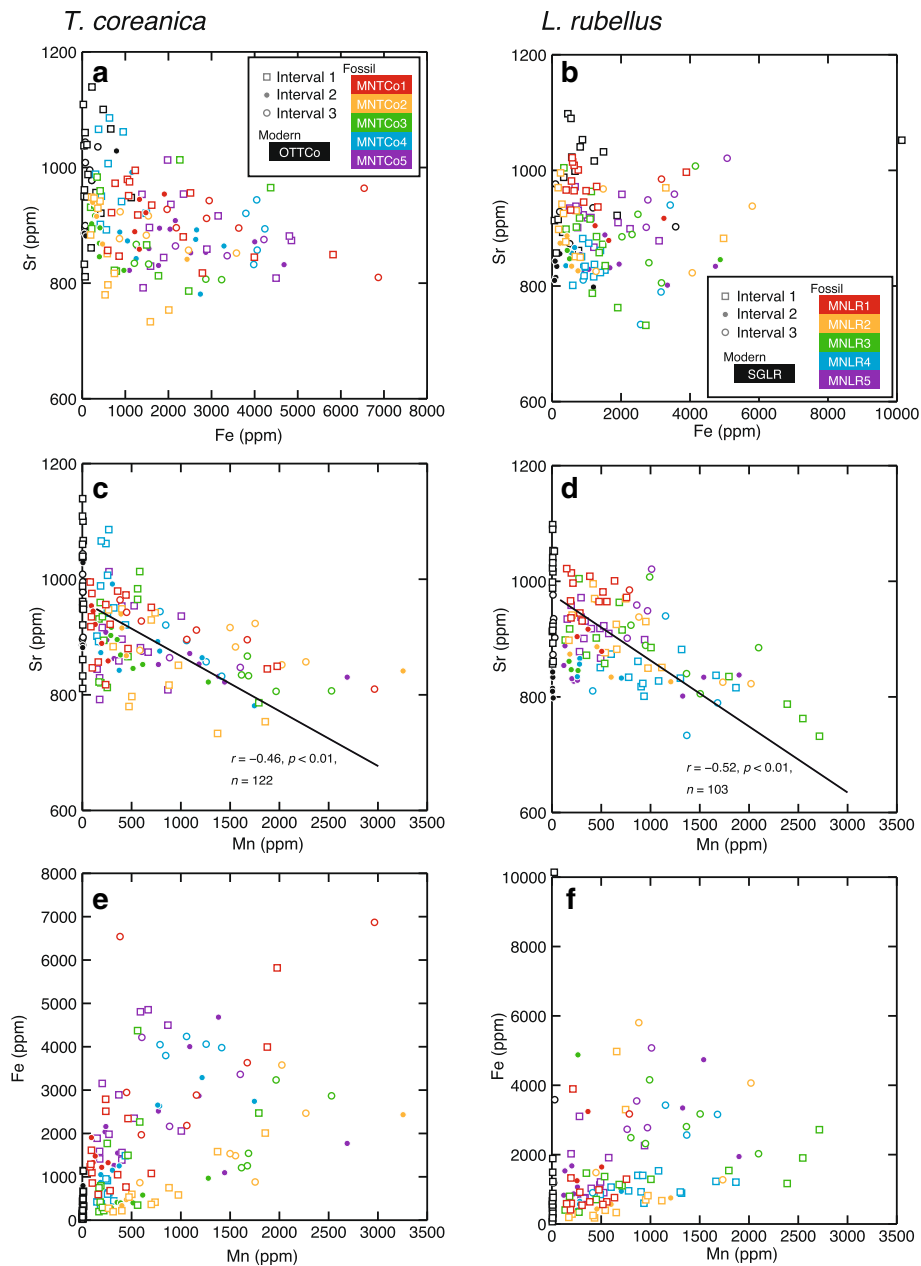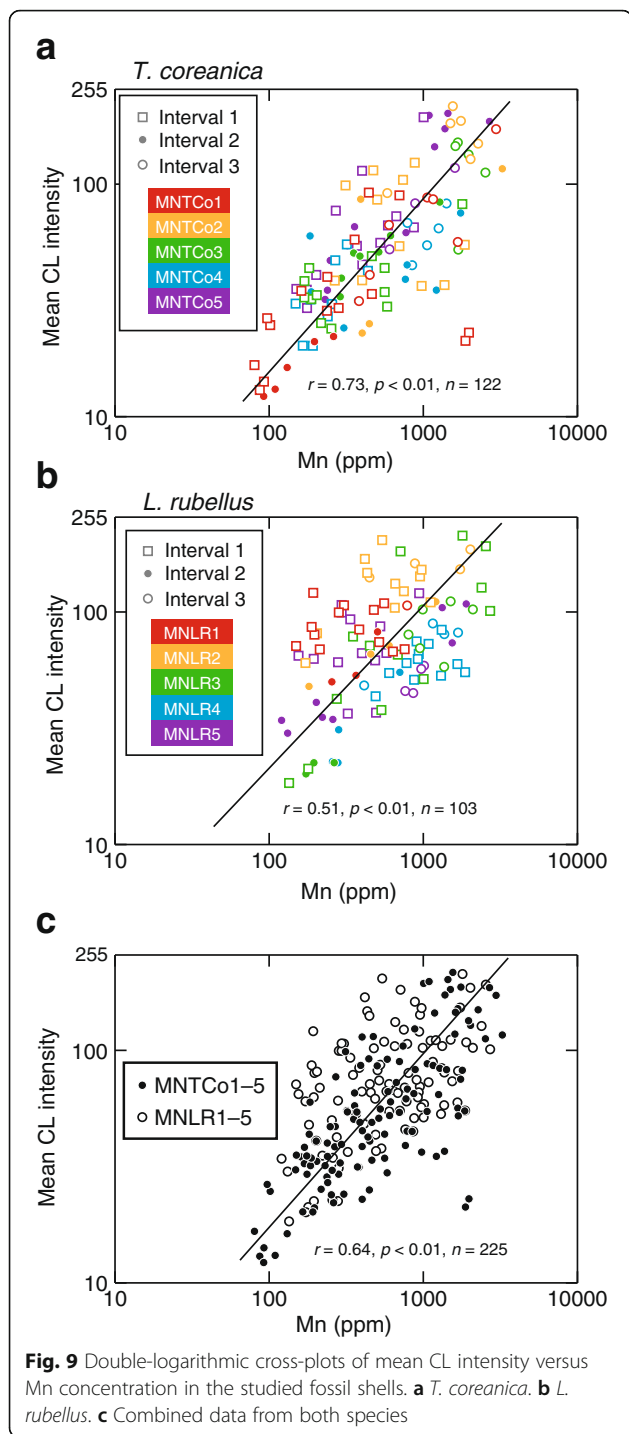
Fig. 8 Cross-plots of minor element (Mn, Fe, and Sr) concentrations in the studied brachiopod shells. The samples were extracted from the modern and fossil *T. coreanica* (**a**, **c**, **e**) and *L. rubellus* (**b**, **d**, **f**) shells

marine invertebrates (Barbin and Gaspard 1995; Barbin 2013; Riechelmann et al. 2016). These bands or lines are the result of biological activity (e.g., bleeding cycles and changes in growth rates) and/or environmental stresses (e.g., input of coastal water, tidal rhythms, and changes in seawater temperature). In the present study, it is difficult to determine the main reason for the difference in the CL intensity between the modern shells of the two species, noting that CL can also be influenced by the measurement conditions (England et al. 2006).

The fossil shells display brighter luminescence than that of the modern shells. No luminescent bands are observed in the fossil shells. The MCLI profiles of the fossil brachiopod shells show statistically significant positive correlations with Mn concentration (*T. coreanica*: $r = 0.73$, $n = 122$, $p < 0.01$; *L. rubellus*: $r = 0.51$, $n = 103$, $p < 0.01$) (Figs. 6a, b and 9a–c). The luminescent regions also correspond to the samples with higher Fe concentrations and lower $\delta^{13}C$ and $\delta^{18}O$ values than those of adjacent non-luminescent regions within an individual shell (Fig. 6a, b),

Fig. 9 Double-logarithmic cross-plots of mean CL intensity versus Mn concentration in the studied fossil shells. **a** *T. coreanica*. **b** *L. rubellus*. **c** Combined data from both species

indicating that these shell portions have been altered by meteoric diagenesis.

The punctae of the fossil brachiopods are partly to fully filled with cement and display bright luminescence (Fig. 4f, h) as has been described in other species (e.g., Takizawa et al. 2017; Casella et al. 2018). This is because the punctae are filled with organic material in live brachiopods (Williams 1997; Pérez-Huerta et al. 2009),

although no such material was observed in the studied modern shells, and void spaces are created during post-mortem decomposition, with subsequent precipitation of diagenetic cements (Garbelli et al. 2016). We conclude that the presence of carbonate cements with extremely high Mn and Fe concentrations in the punctae and inter-fiber spaces is one of the major causes of high concentrations of these elements in diagenetically altered shell portions, as discussed below.

The diagenetic alteration of shell microstructure

The secondary shell layer is composed of calcite fibers, each with a concave outer surface and convex inner surface (Gaspard 1991; Samtleben et al. 2001). However, altered fibers become irregularly shaped and amalgamated with an increased diagenetic alteration. The amalgamation of two or more fibers occurs locally in modern brachiopods, but the outline of such fibers remains defined, which means that pristine amalgamated fibers can be distinguished from diagenetically altered fibers (Samtleben et al. 2001).

Altered shell portions (Additional file 5: Figures S1-2–6 and Additional file 6: Figures S2-2–6) are characterized by low $\delta^{13}C$ and $\delta^{18}O$ values, high Mn and Fe concentrations, and luminescent CL images. In contrast, the well-preserved shell portions exhibit comparatively high $\delta^{13}C$ and $\delta^{18}O$ values, low Mn and Fe concentrations, and weakly luminescent or non-luminescent CL images (Fig. 4f). AFR and AF-PCR are correlated negatively with $\delta^{13}C$ and $\delta^{18}O$ but positively with Mn and Fe concentrations and MCLI in the fossil *T. coreanica* and *L. rubellus* shells (Fig. 10).

Some studies have argued that the impact of in-filling cements in punctae upon the chemical and isotopic composition of shells is negligible because their volume accounts for only a small portion of the shell (e.g., < 10% of a Silurian brachiopod, *Resseralla elegantula*, shells; Samtleben et al. 2001) compared with that of the shell-forming calcite fibers. However, if the isotopic compositions and chemical concentrations of the puncta-filling cements are one or more orders of magnitude greater than those of the shell-forming fibers, the impact of such cements on the geochemistry of spot samples might not be negligible. Here, we assume that the isotopic composition and Mn and Fe concentrations of the puncta-filling cements are identical to those of the cement formed by meteoric diagenesis ($\delta^{13}C = -18‰$, $\delta^{18}O = -7‰$, Mn concentration = 6000 ppm, Fe concentration = 14,000 ppm). The $\delta^{13}C$ values are at least 19‰ lower than those of the fossil shells, and the δ^8O values are 9‰ lower. The Mn concentrations are at least 5000 ppm higher than those of the fossil shells, and Fe concentrations are 12,000 ppm higher. Under this assumption, if the punctae of the studied modern shells are filled with such

Fig. 10 Cross-plots of isotopic composition versus AFR or AF-PCR (**a**, **b**, **e**, and **f**) and of isotopic composition versus MCLI (**c**, **d**, **g**, and **h**) . The gray bar on the *y*-axis indicates a range of $\delta^{13}C$ or $\delta^{18}O$ values of the modern brachiopod shell (OTTCo or SGLR)
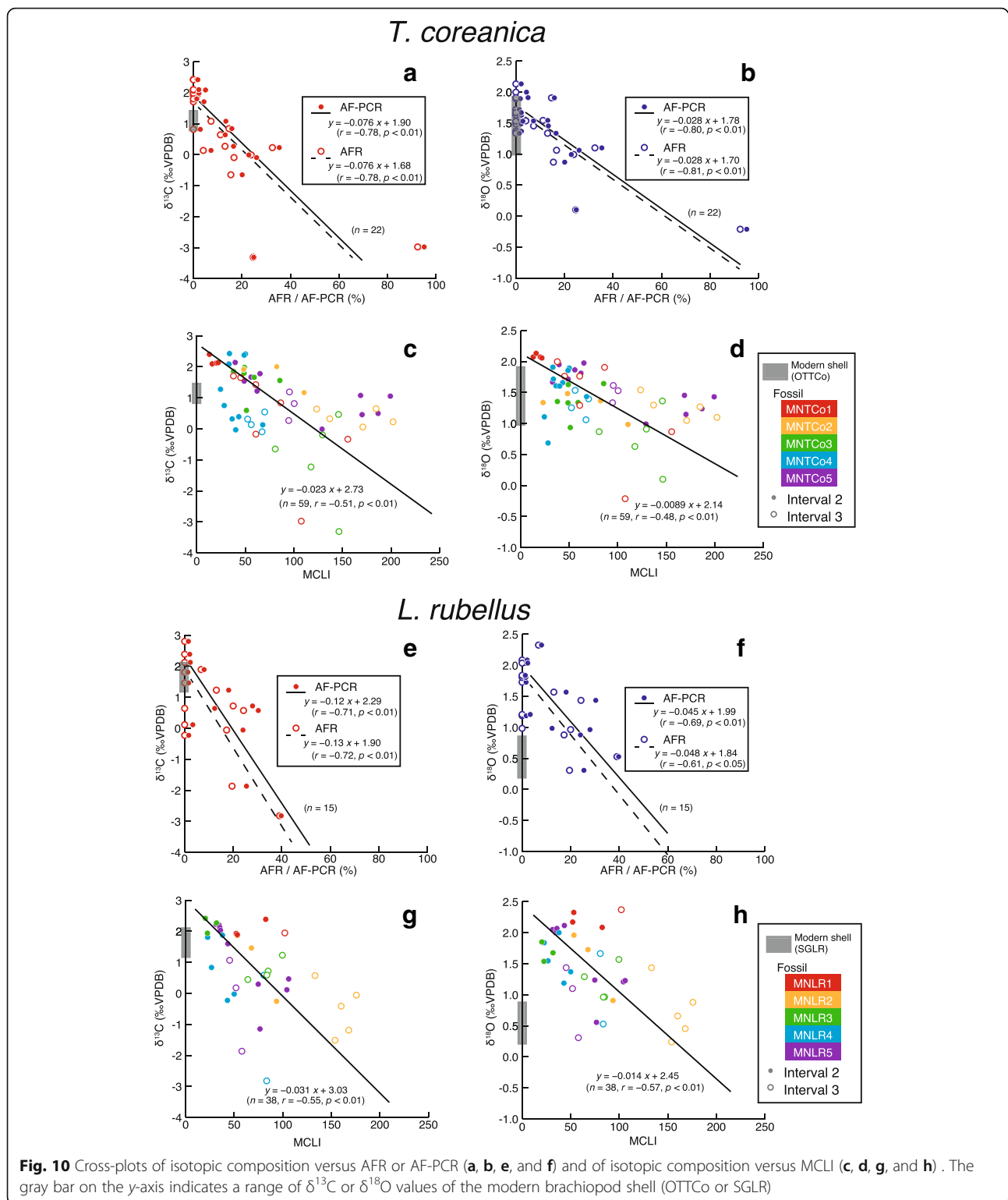
cements and they account for 5% of the shell volumes, then the $\delta^{13}C$ and $\delta^{18}O$ values decrease by ~ 1‰ and ~ 0.4‰, respectively (Table 2). Conversely, the Mn and Fe concentrations increase by ~ 300 and ~ 600 ppm,

respectively. In fact, the punctae account for 1–9% of the fossil *T. coreanica* shell volumes and 1–12% of the *L. rubellus* shell volumes. These indicate that the isotopic composition and chemical concentration of the puncta-

Table 2 Effect of puncta-filling cements to the isotopic composition and minor element concentrations of shell samples. We assume that the isotopic composition and minor element concentrations of the puncta-filling cements are identical to those of the cement formed by meteoric diagenesis. Then, we calculate the isotopic composition and minor element concentrations of the mixtures of shell and puncta-filling cements when the punctae are filled with such cements

	Modern shell	Cement	Puncta filling cements accounting for 5% of the shell volumes		Puncta filling cements accounting for 10% of the shell volumes	
			Shell + cement	Δ*	Shell + cement	Δ*
T. coreanica						
Interval 2						
$\delta^{13}C$ (‰)	1.01 to 1.36	−18	0.06 to 0.39	−0.96	−0.89 to −0.58	−1.92
$\delta^{18}O$ (‰)	1.17 to 1.43	−7	0.76 to 1.01	−0.42	0.35 to 0.59	−0.83
Mn (ppm)	3**	6000	310	300	610	600
Fe (ppm)	70**	14,000	770	700	1500	1400
Sr (ppm)	960**	400	930	−30	900	−60
L. rubellus						
Interval 2						
$\delta^{13}C$ (‰)	1.49 to 1.94	−18	0.52 to 0.94	−0.99	−0.46 to 0.05	−1.97
$\delta^{18}O$ (‰)	0.55 to 0.93	−7	0.17 to 0.53	−0.39	−0.21 to 0.14	−0.78
Mn (ppm)	7**	6000	300	300	600	590
Fe (ppm)	120**	14,000	810	690	1500	1380
Sr (ppm)	820**	400	800	−20	780	−40

*Δ = "shell + cement" − "modern shell"
**Median

filling cements can potentially significantly bias the isotopic composition and minor element concentrations of spot or bulk shell samples.

AF-PCR was correlated more negatively with $\delta^{13}C$ and $\delta^{18}O$ and more positively with Mn and Fe concentrations and MCLI than was AFR (Table 3, Fig. 9). This suggests that the occurrence of puncta-filling cements is one of the major causes of diagenetic modification of isotopic compositions and minor element concentrations. However, it is not clear whether the puncta-filling cements have similar isotopic compositions and minor element concentrations to cements formed by meteoric diagenesis. The punctae of some modern brachiopod shells are luminescent (e.g., Griesshaber et al. 2007; Barbin 2013), indicating that they are filled with carbonate minerals that are enriched in Mn compared with shell calcite. It is deduced that such puncta-filling cements are chemical and/or microbial precipitates formed in a closed reductive space (e.g., Kaźmierczak and Iryu 1999) or biogenic products. As such, the puncta-filling cements in this study might include carbonate minerals of different origins, with likely differences in their isotopic composition and minor element concentrations.

Figure 10 shows the cross-plots of isotopic composition versus AFR/AF-PCR and isotopic composition versus MCLI. The intercepts of these cross-plots can be regarded as the isotopic composition of non-altered brachiopod shells (AFR or AF-PCR = 0, MCLI = 0), theoretically corresponding to the initial isotopic composition of the fossil brachiopod shells. The intercepts are not identical but are close to each other (the difference in $\delta^{13}C$ values is < 1.1‰ and in $\delta^{18}O$ values is < 0.6‰). The intercepts of the $\delta^{18}O$ values of the fossil *T. coreanica* shells are up to 0.5‰ greater than the $\delta^{18}O$ values of the modern shell from Otsuchi Bay. Those of *L. rubellus* are 2‰ greater than the $\delta^{18}O$ values from Sagami Bay. Assuming that the brachiopods occupied similar habitats during the Pliocene to those occupied by their modern counterparts, this indicates the presence of cooler and/or more saline seawater in the Minehama region during the Pliocene compared with that of the modern Otsuchi and Sagami bays. This interpretation is supported by the occurrence of coolwater molluscan species within the outcrop from which the fossil brachiopod shells of this study were collected (MH1; Amano et al. 2011). This suggests that AFR/AF-PCR and MCLI are good indices for quantitatively estimating the extent of diagenetic alteration within brachiopod shells.

The submicron-sized cements in a narrow space in the inter-fiber spaces (Fig. 4i) show the morphological and geochemical features that are common in cements formed during meteoric diagenesis (Tucker and Wright 1990), and the occurrence of such cements is an additional cause of high concentrations of Mn and Fe in diagenetically altered shells.

Table 3 Cross-correlations between geochemical, microstructural and optical signals in the studied fossil brachiopodCross-correlations are calculated between isotope composition ($\delta^{13}C$ and $\delta^{18}O$), minor-element (Mn, Fe, and Mn) concentrations, MCLI, and AFR or AF-PCR of the fossil *Terebratalia coreanica* and *Laqueus rubellus* shells. Coefficient values in brackets are not statistically significant ($p > 0.01$)

	$\delta^{13}C$ (‰ VPDB)	$\delta^{18}O$ (‰ VPDB)	Mn (ppm)	Fe (ppm)	Sr (ppm)	Mean CL intensity (MCLI: 0–255)	Altered fiber and puncta-filling cement ratio (AF-PCR: %)
Fossil T. coreanica and L. rubellus (n = 36)							
$\delta^{13}C$ (‰VPDB)	1						
$\delta^{18}O$ (‰VPDB)	0.9	1					
Mn (ppm)	−0.71	−0.71	1				
Fe (ppm)	−0.51	−0.43	0.61	1			
Sr (ppm)	[0.21]	[0.18]	[−0.42]	[−0.02]	1		
Mean CL intensity (MCLI: 0–255)	−0.53	−0.54	0.77	[0.34]	[−0.23]	1	
Altered fiber and puncta-filling cement ratio (AF-PCR: %)	−0.75	−0.76	0.75	0.6	[−0.15]	0.61	1
Fossil T. coreanica (n = 22)							
$\delta^{13}C$ (‰VPDB)	1						
$\delta^{18}O$ (‰VPDB)	0.9	1					
Mn (ppm)	−0.77	−0.72	1				
Fe (ppm)	[−0.48]	[−0.35]	0.54	1			
Sr (ppm)	0.54	0.55	−0.68	[−0.19]	1		
Mean CL intensity (MCLI: 0–255)	−0.65	−0.64	0.80	[0.20]	−0.47	1	
Altered fiber and puncta-filling cement ratio (AF-PCR: %)	−0.79	−0.81	0.77	0.62	[−0.44]	0.63	1
Fossil L. rubellus (n = 14)							
$\delta^{13}C$ (‰VPDB)	1						
$\delta^{18}O$ (‰VPDB)	0.91	1					
Mn (ppm)	[−0.65]	−0.72	1				
Fe (ppm)	[−0.57]	[−0.56]	0.76	1			
Sr (ppm)	[−0.15]	[−0.20]	[−0.16]	[0.17]	1		
Mean CL intensity (MCLI: 0–255)	[−0.32]	[−0.37]	0.69	[0.62]	[0.05]	1	
Altered fiber and puncta-filling cement ratio (AF-PCR: %)	−0.71	−0.71	0.71	[0.57]	[0.31]	[0.55]	1

The cross-correlation coefficients of isotopic composition, minor element concentration, and MCLI and AF-PCR indices indicating the alteration of shell portions are presented in Table 3. The $\delta^{13}C$ and $\delta^{18}O$ values of the fossil *T. coreanica* and *L. rubellus* shells show moderate to strong negative correlations with Mn concentration, MCLI, and AF-PCR. Mn concentration, MCLI, and AF-PCR were positively correlated. The negative correlation of Fe concentration with isotopic composition is weaker than that of Mn concentration because of the occurrence of localized high Fe concentrations that are more anomalous than the high Mn concentrations. Fe concentration shows a weak (although not statistically significant ($p > 0.01$)) positive correlation with MCLI. Mn and Fe concentrations increase with increased diagenetic alteration and act as an activator (Mn) and a quencher (Fe) for CL images (Machel et al. 1991). The

weak positive correlation of Fe concentration with MCLI indicates that the activator (Mn) acts more efficiently as an activator than Fe does as a quencher. Sr concentration was not correlated significantly with any other features or measures. In summary, shell portions with high Mn concentration, high MCLI, and high AF-PCR generally exhibit low $\delta^{13}C$ and $\delta^{18}O$ values, indicating that these measures are useful for detecting shell portions altered by meteoric diagenesis.

Lithologic control on the diagenetic alteration of brachiopod shells

Our study shows that the four indices commonly used to specify diagenetically altered carbonates—$\delta^{13}C$ and $\delta^{18}O$ values, minor element concentrations, the preservation state of shell microstructure, and cathodoluminescence—are applicable to brachiopod shells. However, it is known

that diagenesis alters the initial paleoenvironmental signals extracted by these indices (Ullmann and Korte 2015). Yamamoto et al. (2017) studied the four indices of fossilized *Kikaithyris hanzawai* shells from the Pleistocene reef complex deposits (Iryu et al. 2006) and showed that although altered fibers are commonly observed in brachiopod shells, the initial isotopic composition can be largely preserved, and luminescent shells cannot always be regarded as having undergone degradation of shell microstructure or isotopic modification by diagenesis. The findings of those authors indicate that CL images are not always sufficient for detecting diagenetic alteration in shells. This is at least partly because of the differences in the diagenetic processes modifying the chemical and isotopic compositions between brachiopod shells embedded in siliciclastic and volcaniclastic deposits and those in carbonate deposits. The geochemistry of brachiopod shells embedded in siliciclastic and volcaniclastic deposits is affected by formation water relatively rich in Mn, which originates from meteoric water. This can explain why diagenetically altered shells are luminescent in CL images, have low $\delta^{13}C$ and $\delta^{18}O$ values, and high Mn concentrations. In contrast, carbonate deposits have limited sources of Mn, except when the deposits are associated with siliciclastics (including paleosols) or volcaniclastics. As such, CL images might not necessarily be useful for the detection of diagenetic alteration of shells in carbonate deposits.

The relationship between the degree of preservation of shell microstructures and the initial isotopic composition has been controversial. It is known that some Paleozoic brachiopods, in spite of their well-preserved shell microstructure, have low $\delta^{13}C$ and $\delta^{18}O$ values, similar to those of diagenetically altered marine carbonate fossils and sparry cements (Rush and Chafetz 1990), or exhibit large variations in isotopic composition caused by a diagenetic alteration (Banner and Kaufman 1994). To explain this conflict, it has been suggested that only large-scale dissolution and subsequent recrystallization of shells can result in isotopic resetting in the per mil range (Wadleigh and Veizer 1992; Qing and Veizer 1994). However, the significantly lower $\delta^{13}C$ and $\delta^{18}O$ values in intervals 2 and 3 of the fossil brachiopod shells compared with those of the modern shells in the present study indicate that the resetting of isotopic values in the per mil range can occur without large-scale dissolution and subsequent recrystallization.

Shell portions in which microstructures are preserved but their initial isotopic composition has been modified present a significant challenge with respect to reconstructing paleoceanographic conditions. Applying and cross-checking multiple criteria to assess diagenetic alteration are required to distinguish between diagenetically altered and unaltered brachiopod shells (Yamamoto et al. 2017).

Conclusions

To estimate the extent of modification in the isotope composition of fossil brachiopod shells with increasing diagenetic alteration, we analyzed $\delta^{13}C$ and $\delta^{18}O$ and three commonly applied indicators of meteoric diagenesis: minor element (Mn, Fe, and Sr) concentrations, cathodoluminescence, and shell microstructure. The samples for these analyses were collected from the inner surfaces of fossil *T. coreanica* and *L. rubellus* (rhynchonellate brachiopod) shells collected from conglomerates of the Tentokuji Formation (Pliocene, 3.85–2.75 Ma) exposed in northeastern Japan. The results of the study can be summarized as follows:

(1) Individual shells of *T. coreanica* and *L. rubellus* can be divided into three intervals (intervals 1–3) based on the shell morphology, each with characteristic chemical and isotopic compositions.

(2) Interval 2 is characterized by relatively small intra-shell and intra-species variations in $\delta^{13}C$ and $\delta^{18}O$ values in both modern and fossil shells. The $\delta^{13}C$ and $\delta^{18}O$ values from this interval of the fossil shells plots as the highest end-member, and these values are therefore likely to be the closest to the initial shell $\delta^{13}C$ and $\delta^{18}O$ values.

(3) Of the three minor elements examined in this study, Mn concentration is the most reliable indicator of diagenetically altered shells. Mn and Fe concentrations in the fossil brachiopod shells are higher than those of the modern shells, displaying large intra-shell and intra-species variations, with several anomalously high localized concentrations. The samples with high Mn and Fe concentrations do not correspond to specific regions of the shells but also exhibit low $\delta^{13}C$ and $\delta^{18}O$ values and strong luminescence. This indicates that the increased Mn concentrations are the result of meteoric diagenetic alteration. The anomalously high Fe concentrations, which are also observed in modern shells, are not necessarily associated with microstructural (dissolution and amalgamation of fibers), optical (strong luminescence on CL images), or isotopic (decreased $\delta^{13}C$ or $\delta^{18}O$ values). This indicates that these anomalously high Fe concentrations are likely not diagenetic products but represent initial concentrations from when the brachiopods were alive. Unlike Mn and Fe concentrations, Sr concentrations in the studied modern and fossil brachiopod shells are similar and their ranges overlap, indicating that Sr concentration in carbonate minerals is not always a good indicator for identifying diagenetic alteration.

(4) We quantified the preservation state of shell microstructure using two indices: altered fiber ratio

(AFR) and altered fiber and puncta-filling cement ratio (AF-PCR). To quantify the degree of luminescence, we measured the mean cathodoluminescence index (MCLI) defined as the mean R value in a particular area of a CL image. The $\delta^{13}C$ and $\delta^{18}O$ values of the fossil brachiopod shells are moderately or strongly negatively correlated with Mn concentration, MCLI, and AF-PCR. Mn concentration, MCLI, and AFR/AF-PCR are positively correlated with each other. Fe concentration shows a weaker negative correlation with isotopic composition than does Mn concentration on account of the occurrence of anomalously high localized Fe concentrations.

Our study provides further evidence that applying and cross-checking multiple criteria to assess diagenetic alteration is the optimal method for distinguishing between diagenetically altered and unaltered brachiopod shells.

Additional files

Additional file 1: Table S1. $\delta^{13}C$ and $\delta^{18}O$ values of the modern *Terebratalia coreanica* (OTTCo) and *Laqueus rubellus* (SGLR) shells. (XLSX 13 kb)

Additional file 2: Table S2. $\delta^{13}C$ and $\delta^{18}O$ value, AFRs (altered fiber ratios), and AF-PCRs (altered fiber and puncta-filling cement ratios) of the fossil *Terebratalia coreanica* (MNTCo1–MNTCo5) and *Laqueus rubellus* (MNLR1–MNLR5) shells. (XLSX 26 kb)

Additional file 3: Table S3. Minor element (Mn, Fe, and Sr) concentrations of the modern *Terebratalia coreanica* (OTTCo) and *Laqueus rubellus* (SGLR) shells. (XLSX 13 kb)

Additional file 4: Table S4. Minor element (Mn, Fe, and Sr) concentrations and MCLIs (mean CL intensities) of the fossil *Terebratalia coreanica* (MNTCo1–MNTCo5) and *Laqueus rubellus* (MNLR1–MNLR5) shells. (XLSX 23 kb)

Additional file 5: Figure S1. Sampling spots, $\delta^{13}C$ and $\delta^{18}O$ values, minor element (Mn, Fe, and Sr) concentrations, mean CL intensities, altered fiber ratios, and altered fiber and puncta-filling cement ratios of the modern (Figure S1-1, OTTCo) and fossil (Figures S1-2–6, MNTCo1–MNTCo5) *T. coreanica* shells. Composite CL images are presented for each shell. SEM and CL images of selected shell portions are also shown. Red and blue arrows indicate local minima in $\delta^{13}C$ and $\delta^{18}O$, respectively. (ZIP 26310 kb)

Additional file 6: Figure S2. Sampling spots, $\delta^{13}C$ and $\delta^{18}O$ values, minor element (Mn, Fe, and Sr) concentrations, mean CL intensities, altered fiber ratios, and altered fiber and puncta-filling cement ratios of the modern (Figure S2-1, SGLR) and fossil (Figures S2-2–6, MNLR1–MNLR5) *L. rubellus* shells. Composite CL images are presented for each shell. SEM and CL images of selected shell portions are also shown. (ZIP 25125 kb)

Additional file 7: Doc. S1. Estimation of $\delta^{13}C$ and $\delta^{18}O$ values of equilibrium calcite. (DOCX 25 kb)

Abbreviations
AF-PCR: Altered fiber and puncta-filling cement ratio; AFR: Altered fiber ratio; CL: Cathodoluminescence; MCLI: Mean CL intensity

Acknowledgements

Authors' contributions
FH, HT, and YI conceptualized and designed this study. FH and YI conducted the fieldwork and sampling. FH, HT, and KY carried out the chemical and isotope analyses. HT and YI collaborated with FH in the interpretation of the data and the construction of the manuscript. All authors read and approved the final manuscript.

Funding

Availability of data and materials
Please contact the corresponding author regarding data requests.

Competing interests
The authors declare that they have no competing interests.

Author details
[1]Department of Earth Science, Graduate School of Science, Tohoku University, Sendai 980-8578, Japan. [2]Department of Earth and Environmental Sciences, Nagoya University, Nagoya 464-8601, Japan.

References
Adams A, Reeve L (1850) Mollusca. Part 1. In: Adams A (ed) The zoology of the voyage of H.M.S. Samarang, Reeve and Benham, London

Amano K, Yoshida A, Sato T (2011) Influence of cooling event at 2.75 ma on the molluscan fauna of the Japan Sea borderland: molluscan fauna from central and northern parts of Akita Prefecture. J Geol Soc Jpn 117:508–522. https://doi.org/10.5575/geosoc.117.508. In Japanese with English abstract

Angiolini L, Darbyshire DPF, Stephenson MH, Leng MJ, Brewer TS, Berra F, Jadoul F (2007) Lower Permian brachiopods from Oman: their potential as climatic proxies. Ear Env Sci Trans Royl Soc Edinburgh 98:327–344. https://doi.org/10.1017/S1755691008075634

Auclair A, Joachimski MM, Lécuyer C (2003) Deciphering kinetic, metabolic and environmental controls on stable isotope fractionations between seawater and the shell of Terebratalia transversa (Brachiopoda). Chem Geol 202:59–78. https://doi.org/10.1016/S0009-2541(03)00233-X

Azmy K, Veizer J, Bassett MG, Copper P (1998) Oxygen and carbon isotopic composition of Silurian brachiopods: implications for coeval seawater and glaciations. Geol Soc Am Bull 110(11):1499–1512. https://doi.org/10.1130/0016-7606(1998)110<1499:OACICO>2.3.CO;2

Banner JL, Kaufman J (1994) The isotopic record of ocean chemistry and diagenesis preserved in non-luminescent brachiopods from Mississippian carbonate rocks, Illinois and Missouri. Geol Soc Am Bull 106:1074–1082. https://doi.org/10.1130/0016-7606(1994)106<1074:TIROOC>2.3.CO;2

Barbin V (2013) Application of cathodoluminescence microscopy to recent and past biological materials: a decade of progress. Mineral Petrol 107:353–362. https://doi.org/10.1007/s00710-013-0266-6

Barbin V, Gaspard D (1995) Cathodoluminescence of recent articulate brachiopod shells. Implication for growth stages and diagenesis evaluation. Geobios 28(Supple 1):39–45. https://doi.org/10.1016/S0016-6995(95)80151-0

Bates NR, Brand U (1991) Environmental and physiological influences on isotopic and elemental compositions of brachiopod shell calcite: implications for the isotopic evolution of Paleozoic oceans. Chem Geol 94:67–78. https://doi.org/10.1016/S0009-2541(10)80018-X

Brand U, Azmy K, Bitner MA, Logan A, Zuschin M, Came R, Ruggiero E (2013) Oxygen isotopes and $MgCO_3$ in brachiopod calcite and a new paleotemperature equation. Chem Geol 359:23–31. https://doi.org/10.1016/j.chemgeo.2013.09.014

Brand U, Logan A, Hiller N, Richardson J (2003) Geochemistry of modern brachiopods: applications and implications for oceanography and paleoceanography. Chem Geol 198:305–334. https://doi.org/10.1016/S0009-2541(03)00032-9

Brand U, Veizer J (1980) Chemical diagenesis of a multicomponent carbonate system-1: minor elements. J Sediment Res 50:1219–1236. https://doi.org/10.1306/212F7BB7-2B24-11D7-8648000102C1865D

Bruckschen P, Oesmann S, Veizer J (1999) Isotope stratigraphy of the European carboniferous: proxy signals for ocean chemistry, climate and tectonics. Chem Geol 161:127–163. https://doi.org/10.1016/S0009-2541(99)00084-4

Casella LA, Griesshaber E, Simonet Roda M, Ziegler A, Mavromatis V, Henkel D, Laudien J, Häussermann V, Neuser RD, Angiolini L, Dietzel M, Eisenhauer A, Immenhauser A, Brand U, Schmahl WW (2018) Micro- and nanostructures reflect the degree of diagenetic alteration in modern and fossil brachiopod shell calcite: a multi-analytical screening approach (CL, FE-SEM, AFM, EBSD). Palaeogeograph Palaeoclimatol Palaeoecol 502:13–30. https://doi.org/10.1016/j.palaeo.2018.03.011

Cusack M, Pérez-Huerta A, EIMF (2012) Brachiopods recording seawater temperature—a matter of class or maturation? Chem Geol 334:139–143. https://doi.org/10.1016/j.chemgeo.2012.10.021

Dall WH (1920) Annotated list of the recent Brachiopoda in the collection of the United States National Museum, with descriptions of thirty-three new forms. Proc US Nat Mus 57:261–377

Endo K (1989) Growth and life mode of a Pleistocene brachiopod, *Kikaithyris hanzawai* (Yabe). Trans Proc Palaeontol Soc Jpn, NS 156:286–290

England J, Cusack M, Paterson NW, Edwards P, Lee MR, Martin R (2006) Hyperspectral cathodoluminescence imaging of modern and fossil carbonate shells. J Geophys Res Biogeosci 111:G03001. https://doi.org/10.1029/2005JG000144

Friedman I, O'Neil JR (1977) Compilation of stable isotope fractionation factors geochemical interest. In: Fleischer M (ed) Data of geochemistry, sixth edition. US Geol Surv Prof Paper 440-KK. US Gov Print Off, Washington D. C

Garbelli C, Angiolini L, Brand U, Jadoul F (2014) Brachiopod fabric, classes and biogeochemistry: implications for the reconstruction and interpretation of seawater carbon-isotope curves and records. Chem Geol 371:60–67. https://doi.org/10.1016/j.chemgeo.2014.01.022

Garbelli C, Angiolini L, Brand U, Shen SZ, Jadoul F, Posenato R, Azmy K, Cao CQ (2016) Neotethys seawater chemistry and temperature at the dawn of the end Permian mass extinction. Gondwana Res 35:272–285. https://doi.org/10.1016/j.gr.2015.05.012

Garbelli C, Angiolini L, Shen S (2017) Biomineralization and global change: a new perspective for understanding the end-Permian extinction. Geology 45:19–22. https://doi.org/10.1130/G38430.1

Gaspard D (1991) Microstructural organisation of the exoskeleton of some articulate brachiopods (Terebratulda, Rhynchonellida). The importance of the calcite granules and the effects of diagenesis. In: Suga S, Nakahara H (eds) Biomineralization 90: mechanisms and phylogeny of mineralization in biological systems. Springer-Verlag, Tokyo

Griesshaber E, Schmahl WW, Neuser R, Pettke T, Blüm M, Mutterlose J, Brand U (2007) Crystallographic texture and microstructure of terebratulide brachiopod shell calcite: an optimized materials design with hierarchical architecture. Am Mineral 92:722–734. https://doi.org/10.2138/am.2007.2220

Grossman EL (1984) Carbon isotopic fractionation in live benthic foraminifera—comparison with inorganic precipitate studies. Geochim Cosmochim Acta 48:1505–1512. https://doi.org/10.1016/0016-7037(84)90406-X

Grossman EL, Mii HS, Yancey TE (1993) Stable isotopes in Late Pennsylvanian brachiopods from the United States: implications for Carboniferous paleoceanography. Geol Soc Am Bull 105:1284–1296. https://doi.org/10.1130/0016-7606(1993)105<1284:SIILPB>2.3.CO;2

Habermann D, Neuser RD, Richter DK (1998) Low limit of Mn^{2+}-activated cathodoluminescence of calcite: state of the art. Sediment Geol 116:13–24. https://doi.org/10.1016/S0037-0738(97)00118-8

Hatai KM (1936a) The geographic distribution of Brachiopoda. Part 1. Recent Brachiopoda of Japan. Bull. Biogeog. Soc. Jpn 6:64–70

Hatai KM (1936b) Neogene Brachiopoda from Japan. Jpn J Geol Geogr 13:283–324

Hatai KM (1938) The tertiary and recent Brachiopoda of northeast Honsyu, Japan. Saito Ho-on Kai Mus Res Bull 16:89–246

Higo S, Callomon P, Goto Y (1999) Catalogue and bibliography of the marine shell-bearing mollusca of Japan. Elle Sci Publ, Yao

Hughes WW, Rosenberg GD, Tkachuck RD (1988) Growth increments in the shell of the living brachiopod *Terebratalia transversa*. Mar Biol 98:511–518

Iryu Y, Matsuda H, Machiyama H, Piller WE, Quinn TM, Mutti M (2006) An introductory perspective on the COREF Project. Island Arc 15:393–406. https://doi.org/10.1111/j.1440-1738.2006.00537.x

Japan Meteorological Agency (2018) Climatological normals in Noshiro (Akita Prefecture) for the period 1998–2010. http://www.data.jma.go.jp/obd/stats/etrn/view/nml_amd_ym.php?prec_no=32&block_no=0183&year=&month=&day=&view=p1. Accessed 1 Dec 2018.

Jelby ME, Thibault N, Surlyk F, Ullmann CV, Harlou R, Korte C (2014) The lower Maastrichtian Hvidskud succession, Møns Klint, Denmark: calcareous nannofossil biostratigraphy, carbon isotope stratigraphy, and bulk and brachiopod oxygen isotopes. Bull Geol Soc Denmark 62:89–104

Jiménez-López C, Romanek CS, Huertas FJ, Ohmoto H, Caballero E (2004) Oxygen isotope fractionation in synthetic magnesian calcite. Geochim Cosmochim Acta 68:3367–3377. https://doi.org/10.1016/j.gca.2003.11.033

Kaźmierczak J, Iryu Y (1999) Cyanobacterial origin of microcrystalline cements from Pleistocene rhodoliths and coralline algal crusts of Okierabu-jima, Japan. Acta Palaeontol Pol 44(2):117–130

Korte C, Jasper T, Kozur HW, Veizer J (2005) δ^{18}O and δ^{13}C of Permian brachiopods: a record of seawater evolution and continental glaciation. Palaeogeogr Palaeoclimatol Palaeoecol 224:333–351. https://doi.org/10.1016/j.palaeo.2005.03.015

Lee X, Hu R, Brand U, Zhou H, Liu X, Yuan H, Yan C, Cheng H (2004) Ontogenetic trace element distribution in brachiopod shells: an indicator of original seawater chemistry. Chem Geol 209:49–65. https://doi.org/10.1016/j.chemgeo.2004.04.029

Logan A (2007) Geographic distribution of extant articulated brachiopods. In Treatise on Invertebrate Paleontology. In: Selden PA (ed) Treatise on invertebrate paleontology, Part H, Brachiopoda (revised), vol.6. Geological Society of America, Boulder, Colorado, and University of Kansas Press, Lawrence, pp 3082–3115

Lowenstam HA (1961) Mineralogy, ^{18}O/^{16}O ratios, and strontium and magnesium contents of recent and fossil brachiopods and their bearing on the history of the oceans. J Geol 69:241–260. https://doi.org/10.1086/626740

Machel HG, Mason RG, Mariano AN, Mucci A (1991) Cause and emission of luminescence in calcite and dolomite. In: Barker CE, Kopp OC (eds) Luminnescent microscopy and spectroscopy: qualitative and quantitative application. SEPM Short Course Note, no. 25, Society for Sedimentary Geology (SEPM), Tulsa, pp 9–25

Marshall JD (1992) Climatic and oceanographic isotopic signals from the carbonate rock record and their preservation. Geol Mag 129:143–160. https://doi.org/10.1017/S0016756800008244

McConnaughey T (1989a) ^{13}C and ^{18}O isotopic disequilibrium in biological carbonates: I. Patterns. Geochim Cosmochim Acta 53:151–162. https://doi.org/10.1016/0016-7037(89)90282-2

McConnaughey T (1989b) ^{13}C and ^{18}O isotopic disequilibrium in biological carbonates: II. In vitro simulation of kinetic isotope effects. Geochim Cosmochim Acta 53:163–171. https://doi.org/10.1016/0016-7037(89)90283-4

McConnaughey TA, Burdett J, Whelan JF, Paull CK (1997) Carbon isotopes in biological carbonates: respiration and photosynthesis. Geochim Cosmochim Acta 61:611–622. https://doi.org/10.1016/S0016-7037(96)00361-4

Mii HS, Grossman EL, Yancey TE (1997) Stable carbon and oxygen isotope shifts in Permian seas of West Spitsbergen-Global change or diagenetic artifact? Geology 25:225–230. https://doi.org/10.1130/0091-7613(1997)025<0227:SCAOIS>2.3.CO;2

Mii HS, Shi GR, Cheng CJ, Chen YY (2012) Permian Gondwanaland paleoenvironment inferred from carbon and oxygen isotope records of brachiopod fossils from Sydney Basin, Southeast Australia. Chem Geol 291:87–103. https://doi.org/10.1016/j.chemgeo.2011.10.002

Mii HS, Shi GR, Wang CA (2013) Late Paleozoic middle-latitude Gondwana environment-stable isotope records from Western Australia. Gondwana Res 24:125–138. https://doi.org/10.1016/j.gr.2012.10.013

Mizota C, Kusakabe M (1994) Spatial distribution of δD-δ^{18}O values of surface and shallow groundwaters from Japan, South Korea and East China. Geochem J 28:387–410. https://doi.org/10.2343/geochemj.28.387

Morrison JO, Brand U (1986) Geochemistry of recent marine invertebrates. Geosci Can 13:237–253

Okai T, Suzuki A, Terashima S, Inoue M, Nohara M, Kawahata H, Imai N (2004) Collaborative analysis of GSJ/AIST geochemical reference materials JCp-1 (coral) and JCt-1 (giant clam). Chikyukagaku (Geochemistry) 38:281–286. https://doi.org/10.14934/chikyukagaku.38.281. In Japanese with English abstract

Parkinson D, Curry GB, Cusack M, Fallick AE (2005) Shell structure, patterns and trends of oxygen and carbon stable isotopes in modern brachiopod shells. Chem Geol 219:193–235. https://doi.org/10.1016/j.chemgeo.2005.02.002

Pérez-Huerta A, Cusack M, McDonald S, Marone F, Stampanoni M, MacKay S (2009) Brachiopod punctae: a complexity in shell biomineralisation. J Struct Biol 167:62–67. https://doi.org/10.1016/j.jsb.2009.03.013

Qing H, Veizer J (1994) Oxygen and carbon isotopic composition of Ordovician brachiopods: implications for coeval seawater. Geochim Cosmochim Acta 58: 4429–4442. https://doi.org/10.1016/0016-7037(94)90345-X

Richardson JR (1975) Loop development and the classification of terebratellacean brachiopods. Palaeontology 18:285–314

Riechelmann S, Mavromatis V, Buhl D, Dietzel M, Eisenhauer A, Immenhauser A (2016) Impact of diagenetic alteration on brachiopod shell magnesium isotope (δ^{26}Mg) signatures: experimental versus field data. Chem Geol 440: 191–206. https://doi.org/10.1016/j.chemgeo.2016.07.020

Romanek CS, Grossman EL, Morse JW (1992) Carbon isotopic fractionation in synthetic aragonite and calcite: effects of temperature and precipitation rate. Geochim Cosmochim Acta 56:419–430. https://doi.org/10.1016/0016-7037(92)90142-6

Rush PF, Chafetz HS (1990) Fabric-retentive, non-luminescent brachiopods as indicators of initial δ^{13}C and δ^{18}O composition: a test. J Sediment Petrol 60: 968–981. https://doi.org/10.1306/D4267659-2B26-11D7-8648000102C1865D

Samtleben C, Munnecke A, Bickert T, Pätzold J (2001) Shell succession, assemblage and species dependent effects on the C/O-isotopic composition of brachiopods—examples from the Silurian of Gotland. Chem Geol 175:61–107. https://doi.org/10.1016/S0009-2541(00)00364-8

Sato T, Higuchi T, Ishii T, Yuguchi S, Amano K, Kameo K (2003) Calcareous nannofossil biostratigraphy of the Upper Pliocene to lowermost Pleistocene distributed in the northern part of Akita Prefecture, Honshu, Japan—with special reference to the late Pliocene paleoceanography event. J Geol Soc Jpn 109:280–292. https://doi.org/10.5575/geosoc.109.280 In Japanese with English abstract

Sato T, Kameo K (1996) Pliocene to Quaternary calcareous nannofossil biostratigraphy of the Arctic Ocean, with reference to late Pliocene glaciation. In: Thiede J, Myhre AM, Firth JV (eds) Proceedings of the Ocean Drilling Program, initial reports, Leg 151. Ocean Drilling Program, College Station, pp 39–59. https://doi.org/10.2973/odp.proc.sr.151.112.1996

Shiino Y, Kitazawa K (2010) Behavior of the Terebratulide brachiopod *Laqueus rubellus*, with special reference to the pedicle function. Jpn J Benthol 26:18–26. https://doi.org/10.5179/benthos.65.18 In Japanese with English abstract

Sippel RF, Glover ED (1965) Structures in carbonate rocks made visible by luminescence petrography. Science 150(3701):1283–1287. https://doi.org/10.1126/science.150.3701.1283

Sowerby GB (1846) Descriptions of thirteen new species of brachiopods. Proc Zool Soc London 14:91–95

Takayanagi H, Asami R, Abe O, Kitagawa H, Miyajima T, Iryu Y (2012) Carbon- and oxygen-isotope compositions of a deep-water modern brachiopod *Campagea japonica* collected off Aguni-jima, Central Ryukyu Islands, southwestern Japan. Geochem J 46:77–87. https://doi.org/10.2343/geochemj.1.0153

Takayanagi H, Asami R, Abe O, Miyajima T, Kitagawa H, Sasaki K, Iryu Y (2013) Intraspecific variations in carbon-isotope and oxygen-isotope compositions of a brachiopod *Basiliola lucida* collected off Okinawa-jima, southwestern Japan. Geochim Cosmochim Acta 115:115–136. https://doi.org/10.1016/j.gca.2013.03.026

Takayanagi H, Asami R, Otate T, Abe O, Miyajima T, Kitagawa H, Sasaki K, Iryu Y (2015) Quantitative analysis of intraspecific variations in the carbon and oxygen isotope compositions of the modern cool-temperate brachiopod *Terebratulina crossei*. Geochim Cosmochim Acta 170:301–320. https://doi.org/10.1016/j.gca.2015.08.006

Takizawa M, Takayanagi H, Yamamoto K, Abe O, Sasaki K, Iryu Y (2017) Paleoceanographic conditions at approximately 20 and 70 ka recorded in Kikaithyris hanzawai (Brachiopoda) shells. Geochim Cosmochim Acta 215:189–213. https://doi.org/10.1016/j.gca.2017.08.002

Tarutani T, Clayton RN, Mayeda TK (1969) The effect of polymorphism and magnesium substitution on oxygen isotope fractionation between calcium carbonate and water. Geochim Cosmochim Acta 33:987–996. https://doi.org/10.1016/0016-7037(69)90108-2

Thomson JA (1927) Brachiopod morphology and genera (Recent and Tertiary). New Zealand Board Sci Art, Manual 7:1–338

Tucker ME, Wright VP (1990) Carbonate Sedimentology. Blackwell, Oxford

Ullmann CV, Campbell HJ, Frei R, Korte C (2014) Geochemical signatures in Late Triassic brachiopods from New Caledonia. New Zealand J Geol Geophys 57: 420–431. https://doi.org/10.1080/00288306.2014.958175

Ullmann CV, Frei R, Korte C, Lüter C (2017) Element/Ca, C and O isotope ratios in modern brachiopods: species-specific signals of biomineralization. Chem Geol 460:15–24. https://doi.org/10.1016/j.chemgeo.2017.03.034

Ullmann CV, Korte C (2015) Diagenetic alteration in low-Mg calcite from macrofossils: a review. Geol Q 59:3–20. https://doi.org/10.7306/gq.1217

Veizer J, Ala D, Azmy K, Bruckschen P, Buhl D, Bruhn F, Carden GAF, Diener A, Ebneth S, Godderis Y, Jasper T, Korte C, Pawellek F, Podlaha OG, Strauss H (1999) ^{87}Sr/^{86}Sr, δ^{13}C and δ^{18}O evolution of Phanerozoic seawater. Chem Geol 161:59–88. https://doi.org/10.1016/S0009-2541(99)00081-9

Wadleigh MA, Veizer J (1992) ^{18}O/^{16}O and ^{13}C/^{12}C in lower Paleozoic articulate brachiopods: implications for the isotopic composition of seawater. Geochim Cosmochim Acta 56:431–443

Wenzel B (2000) Differential preservation of primary isotopic signatures in Silurian brachiopods from Northern Europe. J Sediment Res 70(1):194–209. https://doi.org/10.1306/2DC4090A-0E47-11D7-8643000102C1865D

Williams A (1968) Evolution of the shell structure of articulate brachiopods. Spec Pap Palaeontol 2:1–55

Williams A (1997) Shell structure. In: Kaesler RL (ed) Treatise on invertebrate paleontology part H Brachiopoda [revised 1: introduction]. The Geological Society of America and The University of Kansas Press, Boulder (CO) and Lawrence (KS), pp 267–320

Williams A, Carlson SJ, Brunton CHC, Holmer LE, Popov L (1996) A supra-ordinal classification of the Brachiopoda. Phil Trans Royl Soc London Ser B 351:1171–1193. https://doi.org/10.1098/rstb.1996.0101

Williams A, Rowell AJ (1965) Brachiopod anatomy. In: Moore RC (ed) Treatise on invertebrate paleontology, part H, Brachiopoda. Geological Society of America, Boulder, Colorado, and University of Kansas Press, Lawrence, pp 6–57

Yamamoto K, Asami R, Iryu Y (2010a) Carbon and oxygen isotopic compositions of modern brachiopod shells from a warm-temperate shelf environment, Sagami Bay, central Japan. Palaeogeogr Palaeoclimatol Palaeoecol 291:348–359. https://doi.org/10.1016/j.palaeo.2010.03.006

Yamamoto K, Asami R, Iryu Y (2010b) Within-shell variations in carbon and oxygen isotope compositions of two modern brachiopods from a subtropical shelf environment off Amami-o-Shima, southwestern Japan. Geochem Geophys Geosyst 11:Q10009. https://doi.org/10.1029/2010GC003190

Yamamoto K, Asami R, Iryu Y (2011) Brachiopod taxa and shell portions reliably recording past ocean environments: toward establishing a robust paleoceanographic proxy. Geophys Res Lett 38:L13601. https://doi.org/10.1029/2011GL047134

Yamamoto K, Asami R, Iryu Y (2013) Correlative relationships between carbon- and oxygen- isotope records in two cool-temperate brachiopod species off Otsuchi Bay, northeastern Japan. Paleontol Res 17:12–26. https://doi.org/10.2517/1342-8144-17.1.12

Yamamoto K, Takizawa M, Takayanagi H, Asami R, Iryu Y (2017) Impact of meteoric diagenesis on the geochemistry and microstructure of Pleistocene brachiopod shells from the Ryukyu Islands, southwestern Japan. Island Arc 26:e12217. https://doi.org/10.1111/iar.12217

Zhang J, Quay PD, Wilbur DO (1995) Carbon isotope fractionation during gas-water exchange and dissolution of CO_2. Geochim Cosmochim Acta 59:107–114. https://doi.org/10.1016/0016-7037(95)91550-D

Publisher's Note